



CMS-HIG-21-019

CERN-EP-2024-210
2024/09/23

Measurement of the Higgs boson mass and width using the four-lepton final state in proton-proton collisions at $\sqrt{s} = 13 \text{ TeV}$

The CMS Collaboration^{*}

Abstract

A measurement of the Higgs boson mass and width via its decay to two Z bosons is presented. Proton-proton collision data collected by the CMS experiment, corresponding to an integrated luminosity of 138 fb^{-1} at a center-of-mass energy of 13 TeV is used. The invariant mass distribution of four leptons in the on-shell Higgs boson decay is used to measure its mass and constrain its width. This yields the most precise single measurement of the Higgs boson mass to date, $125.04 \pm 0.12 \text{ GeV}$, and an upper limit on the width $\Gamma_H < 330 \text{ MeV}$ at 95% confidence level. A combination of the on- and off-shell Higgs boson production decaying to four leptons is used to determine the Higgs boson width, assuming that no new virtual particles affect the production, a premise that is tested by adding new heavy particles in the gluon fusion loop model. This result is combined with a previous CMS analysis of the off-shell Higgs boson production with decay to two leptons and two neutrinos, giving a measured Higgs boson width of $3.0^{+2.0}_{-1.5} \text{ MeV}$, in agreement with the standard model prediction of 4.1 MeV. The strength of the off-shell Higgs boson production is also reported. The scenario of no off-shell Higgs boson production is excluded at a confidence level corresponding to 3.8 standard deviations.

Submitted to Physical Review D

1 Introduction

The standard model (SM) of particle physics postulates the existence of a Higgs field responsible for the generation of the masses of fundamental particles. The excitation of this field is known as the Higgs boson (H) [1–7]. The properties of the Higgs boson, observed with a mass of approximately 125 GeV by the ATLAS and CMS Collaborations [8–10] at the CERN LHC, are found to be consistent with the expectations of the SM [11, 12]. The mass of the Higgs boson (m_H) is a free parameter of the model and, since it determines all other Higgs properties, should be measured with as high precision as possible. For example, the Higgs boson couplings to vector bosons strongly depend on the Higgs boson mass and are precisely predicted by the SM. Another important Higgs boson characteristic is its lifetime, predicted by the SM to be 1.6×10^{-22} s, corresponding to a total width (Γ_H) of 4.1 MeV [13], as predicted precisely within the SM for $m_H = 125$ GeV. A deviation from the SM prediction would point to either anomalous Higgs boson couplings or its decay to yet undiscovered particles.

The ATLAS and CMS Collaborations measured the Higgs boson mass to be 125.09 ± 0.24 GeV [14] using $\sqrt{s} = 7$ and 8 TeV proton-proton (pp) collision data from the 2011–2012 data-taking periods (Run 1), corresponding to a total integrated luminosity per experiment of 25 fb^{-1} . This result has been superseded by both collaborations. The ATLAS experiment measured the Higgs boson mass to be $125.11 \pm 0.11(\pm 0.09)$ GeV [15], combining the $H \rightarrow \gamma\gamma$ and $H \rightarrow 4\ell$ ($\ell = e, \mu$) channels from Run 1 and data collected at $\sqrt{s} = 13$ TeV in 2015–2018 (Run 2). The value in parentheses is the statistical uncertainty only. The most recent CMS result, also using the $H \rightarrow \gamma\gamma$ and $H \rightarrow 4\ell$ channels and including Run 1 and 36 fb^{-1} of $\sqrt{s} = 13$ TeV data from 2016, is $m_H = 125.38 \pm 0.14 (\pm 0.11)$ GeV. Measurements from ATLAS and CMS using only the $H \rightarrow 4\ell$ channel and 2016 data are $124.94 \pm 0.18 (\pm 0.17)$ GeV and $125.26 \pm 0.21 (\pm 0.19)$ GeV, respectively.

Considering only on-shell Higgs boson production, CMS set an upper limit on the Higgs boson width $\Gamma_H < 1.10$ GeV at 95% confidence level (CL), limited by the four-lepton invariant mass resolution [16, 17]. Both the ATLAS and CMS experiments have also set limits on Γ_H [18–24] from an off-shell production method [25–27], which relies on the measurement of the ratio of off- to on-shell production rates. Considering both gluon fusion (ggH) and electroweak (EW) processes, the most recent measurements are $\Gamma_H = 3.2^{+2.4}_{-1.7}$ MeV [24] and $\Gamma_H = 4.3^{+3.3}_{-2.5}$ MeV [28] by CMS and ATLAS, respectively. Finally, from an upper limit on the Higgs boson flight distance in the detector, CMS set a lower limit of $\Gamma_H > 3.5 \times 10^{-9}$ MeV at 95% CL [20].

This paper reports an updated CMS measurement of the Higgs boson mass and width using on-shell production and the $H \rightarrow 4\ell$ decay. The data sample includes 138 fb^{-1} of pp collision data at $\sqrt{s} = 13$ TeV collected in 2016–2018, in combination with the Run 1 data. Compared to the previous CMS on-shell Higgs boson measurement in this channel [17], the statistical and systematic uncertainties affecting m_H have been reduced by including the beam spot in a refit of the muon tracks; adopting an improved event categorization procedure; and performing a detailed study of the lepton momentum scale and resolution.

A measurement of the relative off- and on-shell Higgs boson production offers direct information about Γ_H [25–27]. For each Higgs boson production mechanism j , with subsequent decay to four leptons, the on- and off-shell cross sections σ_j are proportional to

$$\sigma_j^{\text{on-shell}} \propto \mu_j^{\text{on-shell}} \quad \text{and} \quad \sigma_j^{\text{off-shell}} \propto \mu_j^{\text{on-shell}} \Gamma_H, \quad (1)$$

where $\mu_j^{\text{on-shell}}$ is the on-shell signal strength, defined as the ratio of the observed number of on-shell four-lepton events relative to the SM expectation. The signal strength is denoted as

μ_F for Higgs boson production mechanisms driven by fermion couplings, i.e., production via ggH or in association with a $t\bar{t}$ ($t\bar{t}H$) or $b\bar{b}$ pair ($b\bar{b}H$). For EW production, i.e., production via vector boson fusion (VBF) or in association with a W or Z boson (VH), the ratio is denoted as μ_V . Contrary to on-shell in both gluon fusion and EW production, there is sizable destructive interference between the Higgs boson signal and the nonresonant four-lepton production in the off-shell region [26, 29]. This interference is crucial for maintaining unitarity and scales with $\sqrt{\mu_j^{\text{on-shell}} \Gamma_H}$.

In the described technique for measuring Γ_H , it is anticipated that the ratio of the couplings governing off- and on-shell production matches the SM prediction. In particular, it is assumed that the dominant production mechanism is ggH rather than quark-antiquark annihilation. The dominance of the ggH production mechanism has been thoroughly tested in the on-shell regime [12, 13]. It is also assumed that beyond-SM particles do not make significant contributions to the ggH loop within the mass range considered by the analysis. In this paper, we explicitly test this assumption for the first time through a joint off- and on-shell analysis and find that the Γ_H constraints are not substantially altered. In our previous off-shell analyses [23, 24], we evaluated the anomalous contributions to the HVV vertex (where V denotes a W boson, Z boson, or γ) in both EW production and Higgs boson decay. We found that these potential contributions did not significantly affect the Γ_H bounds. It is also assumed that no beyond-SM particles, such as higher-mass resonances, significantly contribute within the mass range investigated by the analysis. However, such resonances would typically increase the yield of events at higher masses, which is not supported by our measurement, and no such resonances have been found in a direct search [30]. These tests do not address every possible scenario that could impact the measurement of the width, but a violation of any of the above assumptions would, by itself, indicate the presence of physics beyond the SM.

The Higgs boson width may deviate from the SM expectation of 4.1 MeV [13] if the Higgs boson has non-SM decay channels, or if the known decay modes have non-SM rates. Therefore, the direct measurement of the Higgs boson width complements searches for Higgs boson decays to invisible or undetected particles and measurements of the Higgs boson couplings to the known SM particles. For example, if the Higgs boson decays into a pair of unknown particles, potentially candidates for dark matter, this would increase the predicted Higgs boson width but would not introduce a bias into the measurement technique.

2 The CMS detector

The central feature of the CMS apparatus is a superconducting solenoid of 6 m internal diameter, providing a magnetic field of 3.8 T. Within the solenoid volume are a silicon pixel and strip tracker, a lead tungstate crystal electromagnetic calorimeter (ECAL), and a brass and scintillator hadron calorimeter (HCAL), each composed of a barrel and two endcap sections. Forward calorimeters extend the pseudorapidity coverage provided by the barrel and endcap detectors. Muons are reconstructed in gas-ionization detectors embedded in the steel flux-return yoke outside the solenoid. More detailed descriptions of the CMS detector, together with a definition of the coordinate system used and the relevant kinematic variables, can be found in Refs. [31, 32].

Events of interest are selected using a two-tiered trigger system. The first level, composed of custom hardware processors, uses information from the calorimeters and muon detectors to select events at a rate of around 100 kHz within a fixed latency of about 4 μ s [33]. The second level, known as the high-level trigger, consists of a farm of processors running a version of the

full event reconstruction software optimized for fast processing, and reduces the event rate to around 1 kHz before data storage [34].

The primary vertex is taken to be the vertex corresponding to the hardest scattering in the event, evaluated using tracking information alone, as described in Section 9.4.1 of Ref. [35].

The electron momentum is estimated by combining the energy measurement in the ECAL with the momentum measurement in the silicon tracker. The transverse momentum (p_T) resolution for electrons with $p_T \approx 45\text{ GeV}$ from $Z \rightarrow ee$ decays ranges from 1.6 to 5%. It is generally better in the barrel region than in the endcaps, and also depends on the bremsstrahlung energy emitted by an electron as it traverses the material in front of the ECAL [36, 37].

Muons are measured in the pseudorapidity range $|\eta| < 2.4$, with detection planes made using three technologies: drift tubes, cathode strip chambers, and resistive plate chambers. The single-muon trigger efficiency exceeds 90% over the full η range, and the efficiency to reconstruct and identify muons is greater than 96%. Matching muons to tracks measured in the silicon tracker results in a relative transverse momentum resolution, for muons with p_T up to 100 GeV, of 1% in the barrel and 3% in the endcaps. The p_T resolution in the barrel is better than 7% for muons with p_T up to 1 TeV [38].

3 Data and simulated samples

The data sample used in this analysis corresponds to integrated luminosities of 36.3, 41.5, and 59.8 fb^{-1} collected in 2016, 2017, and 2018, respectively, for a total of 138 fb^{-1} at a center-of-mass energy of 13 TeV. Events are selected online using the same set of triggers as adopted in Ref. [39]. They require the presence of at least one lepton (either muon or electron), or up to three leptons with relaxed p_T conditions. The trigger efficiency relative to the offline selection is found to be larger than 99%, measured in data using 4ℓ events collected by the single-lepton triggers. It agrees with the expectation from simulation at permille precision. Monte Carlo simulations are used to model signal processes, which involve the Higgs boson and background processes.

On-shell Higgs boson production through ggH is simulated using the POWHEG 2.0 [40–46] event generator at next-to-leading order (NLO) in quantum chromodynamics (QCD). Simulation with the MINLO [47] program at NLO in QCD is used for the evaluation of systematic uncertainties related to the modeling of jets produced in association with the Higgs boson. Modeling of associated jet activity in gluon fusion simulation is important for categorization of events across a wide range of four-lepton invariant masses for the Higgs boson off-shell analysis.

On-shell Higgs boson production through VBF, in association with a W or Z boson, or with a $t\bar{t}$ pair, is simulated using both POWHEG 2.0 at NLO in QCD and JHUGEN 7.3.0 [48–52] at leading order (LO) in QCD. Production in association with a $b\bar{b}$ pair or a single top quark is simulated only at LO in QCD with JHUGEN. In the VBF, VH, and $t\bar{t}H$ production modes, the JHUGEN and POWHEG simulations are explicitly compared after parton showering, and no significant differences are found in the kinematic observables. Both on- and off-shell Higgs boson production are simulated following Refs. [23, 24]. Therefore, the JHUGEN simulation is adopted to describe kinematic distributions in the VBF, VH, $t\bar{t}H$, $b\bar{b}H$, and tqH production mechanisms in the on-shell region, with the expected yields taken from the higher-order POWHEG simulation. The considered VH process does not include $gg \rightarrow ZH$ production, which is expected to contribute only about 5% of the VH cross section [13], and is therefore neglected in this

analysis.

The samples modeling off-shell production include interference effects between diagrams with and without the Higgs boson in the propagator. The $gg \rightarrow ZZ / Z\gamma^* \rightarrow 4\ell$ process is simulated with MCFM 7.0.1 [27, 53–55], which is integrated into the JHUGEN generator framework, which is also used to model the vector boson scattering and triple-gauge-boson (VVV) backgrounds, the EW signal, and their interference. The background is modeled using the MCFM matrix elements. The JHUGEN framework enables the incorporation of anomalous interactions involving the Higgs boson or gauge bosons in both ggH and EW production processes. The simulation of the EW processes is validated by comparing its results to those obtained with the PHANTOM 1.3 generator [56]. All off-shell production simulations are conducted at LO in QCD, with higher-order corrections included through a K factor, as described later.

The MELA [48–52] package contains a library of matrix elements from JHUGEN for the simulation of the signal channel and from MCFM for the background, which enables further reweighting of the generated off-shell samples, as discussed in the following. The POWHEG program is used to simulate wide resonances with masses ranging from 115 GeV to 3 TeV produced in ggH, VBF, or VH, and the JHUGEN program simulates their decay to four leptons. The events from the POWHEG + JHUGEN simulation are reweighted using the MELA package to model off-shell Higgs boson production distributions, as an alternative approach to the direct off-shell simulation discussed above. The two approaches are complementary and allow us to apply mutual cross-checks. Both approaches use the same LO matrix elements available in the MELA package based on the JHUGEN framework. Reweighting of simulated high-mass POWHEG + JHUGEN events allows the modeling to start from NLO calculations of the SM signal hard-scattering production integrated with the parton shower simulation, compared to integrating LO production of direct off-shell samples. This gives better modeling of the associated jet activity in the events. Furthermore, introducing additional reweighting based on the LO matrix elements would lead to more complexity and internal inconsistencies in the QCD order, which is utilized in the reweighting to obtain both the background and interference predictions.

In the gluon fusion process, the factorization and renormalization scales are allowed to run by equating them to $m_{4\ell}/2$. To include higher-order QCD corrections, signal cross section calculations are performed at LO, NLO, and next-to-NLO (NNLO), using the MCFM and HNNLO 2 programs [57–59] with a narrow-width approximation, for a wide range of masses covering both on- and off-shell ranges. The ratios between the NNLO and LO cross section values, called the NNLO-to-LO K factors, are used to reweight [13] the $m_{4\ell}$ distributions from the MCFM and JHUGEN simulations at LO in QCD. A uniform K factor of 1.10 is applied across the entire $m_{4\ell}$ range to normalize the Higgs boson production cross section via gluon fusion to the predictions for $m_{4\ell} \approx 125$ GeV at next-to-NNLO ($N^3\text{LO}$) in QCD [13]. The $m_{4\ell}$ distributions obtained from the POWHEG + JHUGEN simulation of the ggH process are reweighted with the NNLO-to-NLO K factors.

While the NNLO-to-LO K factor calculation is directly applicable to the signal cross section, it is only approximate for the $gg \rightarrow ZZ$ background and its interference with the signal. An approximate NLO calculation [60–63] is available for the background and the interference. Using the results of this NLO calculation instead of the values from the simulation programs leads to an increase in the NNLO-to-NLO K factor for the interference close to the $m_{4\ell}$ value corresponding to the kinematic threshold for two on-shell Z bosons. However, the NNLO-to-NLO K factors for the background and interference are consistent with that for the signal within approximately 10% in the relevant mass range for this analysis of $m_{4\ell} > 220$ GeV. We therefore multiply the background and interference contributions by the same NNLO-to-LO K

factor and uniform N³LO correction, both calculated for the signal and including associated uncertainties. We introduce an additional 10% uncertainty associated with this factor for the background and the square root of this value for the interference.

The q \bar{q} → 4 ℓ background simulation is performed at NLO in QCD and LO in the EW theory with POWHEG. The fully differential cross section for this process has been computed at NNLO in QCD [64], and the NNLO-to-NLO K factor as a function of $m_{4\ell}$ has been applied to the POWHEG sample. This K factor is 1.1 at $m_{4\ell} = 125$ GeV and it varies from 1.0 to 1.2 in the $m_{4\ell} < 500$ GeV range. The uncertainty due to missing EW corrections in the region $m_{4\ell} < 2m_Z$ is expected to be small compared to the uncertainties in the QCD calculation. An EW NLO-to-LO K factor [65] is applied to two on-shell Z bosons. This K factor depends on $m_{4\ell}$, decreasing from unity (close to 125 GeV) to ≈0.9 (in the $m_{4\ell} > 500$ GeV range). The uncertainty in the latter is the dominant uncertainty for the off-shell width measurement and is applied as a function of $m_{4\ell}$. In the on-shell region, the EW background from the VVV, t \bar{t} VV, and t \bar{t} V processes is generated with MADGRAPH5_aMC@NLO [66].

All signal and background event generators are interfaced with the PYTHIA 8.320 program [67] to simulate multiparton interactions, parton showering, and hadronization. The CUETP8M1 and CP5 tunes [68, 69] are applied in simulating the 2016 and 2017–2018 data-taking periods, respectively. The NNPDF 3.1 parton distribution functions [70] are used for all simulated samples. Simulated events include the contribution from additional pp interactions within the same or adjacent bunch crossings (pileup) and are weighted to reproduce the pileup distribution observed in data. The generated events are further processed through a detailed simulation of the CMS detector based on GEANT4 [71].

4 Event reconstruction and selection

The event reconstruction is based on the particle-flow (PF) algorithm [72]. This algorithm aims to reconstruct and identify each individual particle in an event, with an optimized combination of information from the various elements of the CMS detector. The energy of photons is obtained from the ECAL measurement. The energy of electrons is determined from a combination of the electron momentum at the primary vertex as determined by the tracker, the energy of the corresponding ECAL cluster, and the energy sum of all bremsstrahlung photons spatially compatible with originating from the electron track. The energy of muons is obtained from the curvature of the corresponding track. The energy of charged hadrons is determined from a combination of their momentum measured in the tracker and the matching ECAL and HCAL energy deposits, corrected for the response function of the calorimeters to hadronic showers. Finally, the energy of neutral hadrons is obtained from the corresponding corrected ECAL and HCAL energies.

Muons with $p_T > 5$ GeV are reconstructed within the geometrical acceptance, corresponding to the region $|\eta| < 2.4$, by combining information from the silicon tracker and the muon systems [38]. The muons are selected among the reconstructed muon track candidates by applying quality requirements on the track in both the muon and silicon tracker systems, and demanding small energy deposits in the calorimeters. A relative muon isolation variable is defined as

$$\mathcal{I}^\mu \equiv \left(\sum p_T^{\text{charged}} + \max [0, \sum p_T^{\text{neutral}} + \sum p_T^\gamma - p_T^{\text{PU}}] \right) / p_T, \quad (2)$$

where p_T is the muon transverse momentum, and p_T^{charged} , p_T^{neutral} , and p_T^γ are the transverse momentum of charged hadrons, neutral hadrons, and photons, respectively, within an cone

radius of $\Delta R = 0.3$ around the muon direction at the primary vertex.

Here, $\Delta R(i,j) \equiv \sqrt{(\eta^i - \eta^j)^2 + (\phi^i - \phi^j)^2}$, where ϕ is the azimuthal angle, and in this case i refers to the hadron or photon, and j to the muon. Since the isolation variable is particularly sensitive to energy deposits from pileup interactions, a contribution p_T^{PU} from pileup is subtracted from the isolation parameter, as shown in Eq. (2). It is defined as the p_T sum of all charged hadrons i not originating from the primary vertex $p_T^{\text{PU}} = 0.5 \sum_i p_T^{i,\text{PU}}$, where the 0.5 factor accounts for the different fraction of charged and neutral hadrons [73]. A requirement of $\mathcal{I}^\mu < 0.35$ is placed on each muon in the event.

Photons from final-state radiation are reconstructed using the PF algorithm [72]. Isolated photons with $p_T > 2\text{ GeV}$, $|\eta| < 2.4$, and $\mathcal{I}^\gamma < 1.8$, are associated with the closest lepton (either muon or electron) in the event. Photons that do not satisfy the requirements $\Delta R(\gamma, \ell)/(p_T^\gamma)^2 < 0.012\text{ GeV}^{-2}$ and $\Delta R(\gamma, \ell) < 0.5$ are discarded. If more than one photon candidate fulfils the above conditions, the one with the lowest value of $\Delta R(\gamma, \ell)/(p_T^\gamma)^2$ with respect to the given lepton is retained. Photons passing the above criteria are excluded from the computation of the relative isolation parameter.

Electrons with $p_T > 7\text{ GeV}$ are reconstructed within the geometrical acceptance, corresponding to the pseudorapidity region $|\eta| < 2.5$ [36]. They are identified using a multivariate discriminant, which includes observables sensitive to the emission of bremsstrahlung along the electron trajectory, the geometrical and momentum-energy matching between the electron trajectory and the associated cluster in the ECAL, the shape of the electromagnetic shower in the ECAL, and variables that discriminate against electrons originating from photon conversions. The isolation parameter sums for electrons, defined similarly as for muons, are included in the multivariate discriminant. This information is used to discriminate between prompt leptons from Z boson decays and those arising from EW decays of hadrons within jets. The package XGBOOST [74] is used to train and optimize this multivariate discriminant. The training is performed with simulated events that are not used at any other stage of the analysis. Separate trainings are performed for the three different data-taking periods [75]. Electrons from photon conversions and muons from in-flight decays of hadrons are rejected if the ratio of their impact parameter in three dimensions, computed with respect to the primary vertex position, to their uncertainty is greater than four.

The reconstruction and selection efficiencies for prompt leptons in both data and simulation have been estimated using a tag-and-probe technique [76] based on samples of Z boson events. The ratio of the efficiencies measured in data and simulation is used to rescale the yields of selected events in the simulated samples. In addition, Z boson events have been used to calibrate the momentum scale and resolution of electrons and muons in bins of different kinematic variables [37, 77].

In the selection of Higgs boson candidates, four prompt and isolated leptons are required following the prescription above. One of the leptons must have $p_T > 20\text{ GeV}$ and at least one of the remaining leptons satisfy $p_T > 10\text{ GeV}$. The Z boson candidates are constructed from e^+e^- or $\mu^+\mu^-$ pairs whose invariant mass is in the range $12\text{--}120\text{ GeV}$. The dilepton pairs are then combined to form the Higgs boson candidate. In the following, Z_1 denotes the pair with the mass closest to the nominal Z boson mass, while Z_2 refers to the remaining one. Four possible combinations are considered and treated separately: 4μ , $4e$, $2e2\mu$, and $2\mu2e$, where the mixed-flavor final states are separated based on the decay of Z_1 . The four possible combinations have different four-lepton mass resolutions (largely driven by whether the Z_1 is formed from 2μ or $2e$) and different amounts of reducible background (largely driven by whether the Z_2 decays to 2μ or $2e$). None of the above differences between the flavor channels affect the off-shell Higgs

boson analysis and therefore all flavor channels are combined in that measurement. Signal candidates must satisfy $m_{4\ell} > 70 \text{ GeV}$. If more than one Higgs boson candidate can be formed in the event, the one with the highest value of the kinematic discriminant $\mathcal{D}_{\text{bkg}}^{\text{kin}}$, defined in Section 6, is retained, unless these candidates consist of the same four leptons. In this case, the candidate with the Z_1 invariant mass closest to the nominal Z boson mass is retained.

In the off-shell analysis, events are further categorized based on the jets associated with the Higgs boson candidate. The jets are clustered using the anti- k_T jet finding algorithm [78, 79] with a distance parameter of 0.4. The jet momentum is determined as the vector sum of all particle momenta in the jet. Jets must satisfy $p_T > 30 \text{ GeV}$ and $|\eta| < 4.7$ and must be separated from all selected lepton candidates and any selected final-state radiation photons by demanding $\Delta R(\ell/\gamma, \text{jet}) > 0.4$. Jets originating from the hadronization of b quarks are identified using the DeepCSV algorithm [80], which combines information on impact parameter significance, the secondary vertex, and jet kinematic variables. The use of this identification is described in Section 6.

5 Lepton momentum measurement and four-lepton mass resolution

Once an event is selected in the Higgs boson mass and on-shell width measurements, beam spot information is used to improve the $m_{4\ell}$ resolution. In this approach (denoted as BS in the following), the beam spot position is included as a common point in the reconstruction of the tracks from the Higgs boson decay. While muon kinematic parameters such as p_T are recalculated after implementing this constraint, electron kinematic parameters are not modified. This is because the electron momentum is determined mostly by the energy measurement in the ECAL, rather than from the track curvature. Thus, applying the beam spot constraint does not change the momentum measurement. In the final states involving muons, the BS constraint improves the $m_{4\ell}$ resolution by about 3–8%, mostly depending on the flavor of the leptons originating from Z_1 .

Once the BS approach is applied, an important variable, the event-by-event four-lepton mass uncertainty ($\delta m_{4\ell}$), is introduced. Individual lepton momentum uncertainty (per-lepton uncertainty in the following) is obtained from the algorithms used to estimate lepton momenta. For muons, the full covariance matrix is obtained from the muon track fit, and the uncertainty in the muon direction is assumed to be negligible. For the electrons, the momentum uncertainty is estimated from the combination of the ECAL and silicon tracker measurements, neglecting the uncertainty in the track direction. The per-lepton momentum uncertainty is then propagated to the $m_{4\ell}$ to predict $\delta m_{4\ell}$. Each $\delta m_{4\ell}^i$ corresponding to individual lepton momentum variation is calculated separately. The total per-event uncertainty $\delta m_{4\ell}$ is obtained as the quadrature sum of the four individual $\delta m_{4\ell}^i$.

This invariant mass uncertainty is decreased by applying correcting factors to the momentum uncertainty. These corrections are derived for muons in several $|\eta|$ bins, and for electrons in bins of $\delta p_T/p_T$ vs. $|\eta|$. The 2ℓ invariant mass distribution is used to extract these corrections. The mass distribution is fit in two steps with a convolution of a Breit-Wigner function (that describes the intrinsic shape of the Z boson resonance) with a double-sided Crystal Ball function [81] (to describe the detector effects), plus an exponential function (used to describe the background). The first step is used to estimate all the parameters in the fit function, while the correction to the momentum uncertainty is determined in the second step. After the corrections are extracted, a closure test between the predicted and measured invariant mass resolutions is

performed.

To further improve the $m_{4\ell}$ resolution, a kinematic fit is also performed using a mass constraint on the intermediate on-shell Z resonance, with an approach similar to the one described in Ref. [17]. For a 125 GeV Higgs boson, the selected Z_1 is mostly on-shell, while the m_{Z_2} invariant mass distribution is broad and the width is much larger than the detector resolution. When considering the Higgs boson mass measurement, the expected gain in resolution comes from refitting Z_1 . Thus, it is possible to reevaluate the p_T of the two leptons forming Z_1 , using the constraint that the reconstructed invariant mass of the Z boson candidates must follow the true shape of the Z boson. In every event, the lepton momenta are adjusted using the likelihood function

$$\mathcal{L}(p_T^1, p_T^2 | p_T^{\text{reco}1}, \sigma^1, p_T^{\text{reco}2}, \sigma^2) = \text{Gauss}(p_T^{\text{reco}1} | p_T^1, \sigma^1) \text{Gauss}(p_T^{\text{reco}2} | p_T^2, \sigma^2) \mathcal{L}(m_{12} | m_Z, m_H),$$

where $p_T^{\text{reco}1}$ and $p_T^{\text{reco}2}$ are the reconstructed transverse momenta of the two leptons forming the Z_1 , σ^1 and σ^2 are the per-lepton resolutions (uncertainties in the p_T measurements, corrected using the method described above), p_T^1 and p_T^2 are the observables under optimization, and m_{12} is the invariant mass calculated from p_T^1 and p_T^2 . Finally, $\mathcal{L}(m_{12} | m_Z, m_H)$ is the likelihood function given the true shapes of m_{Z_1} and of the 125 GeV Higgs boson. For each event, the likelihood is maximized and the p_T values of the refitted leptons are updated.

For the Higgs boson off-shell production, the $m_{4\ell}$ distribution is much broader than the $m_{4\ell}$ resolution, and, therefore, improvements in the treatment of the lepton momentum uncertainties are not applied. Figure 1 shows the $m_{4\ell}$ distribution inclusively for all the four-lepton states (upper plot) and separately for the four individual final states. Expectations for the signal and background contributions are shown as stacked histograms. The yields from the signal and ZZ backgrounds are estimated from simulation assuming SM cross sections, while the Z + X background yield is estimated from data. More details are given in Sections 7 and 8. Figure 2 displays the distribution of the relative per-event mass uncertainty of the four-lepton system ($\delta m_{4\ell} / m_{4\ell}$) in the inclusive final state with $105 < m_{4\ell} < 140$ GeV. This variable is used to categorize events in the on-shell region according to their invariant mass resolution. The categorization is performed by defining nine mutually exclusive bins with an equal number of signal events in each. Since each final state has a different resolution that also varies across data-taking periods, the bin boundaries are determined independently per final state and per data-taking year. Figure 3 plots the observed and predicted yields of four-lepton events as a function of $\delta m_{4\ell} / m_{4\ell}$ bin for the $105 < m_{4\ell} < 140$ GeV invariant mass range. This approach improves the precision of the Higgs boson mass measurement by about 10%.

6 Kinematic discriminants and off-shell event categorization

The reconstructed four-lepton events and their associated jets, where relevant, can be described with several observables using the kinematic features of the Higgs boson decay and associated particles. It is a challenging task to perform an optimal analysis in a large multidimensional phase space. There are up to 13 observables in the set Ω that describe the Higgs boson kinematic distributions in the $2 \rightarrow 6$ process of collision of two protons and the production of four leptons and two associated jets. The MELA approach is designed to reduce the number of observables to the minimum while retaining all essential information. In this method, optimal discriminators are defined through the utilization of matrix element likelihood calculations [48–52]. Two types of discriminants are defined for each of the Higgs boson production

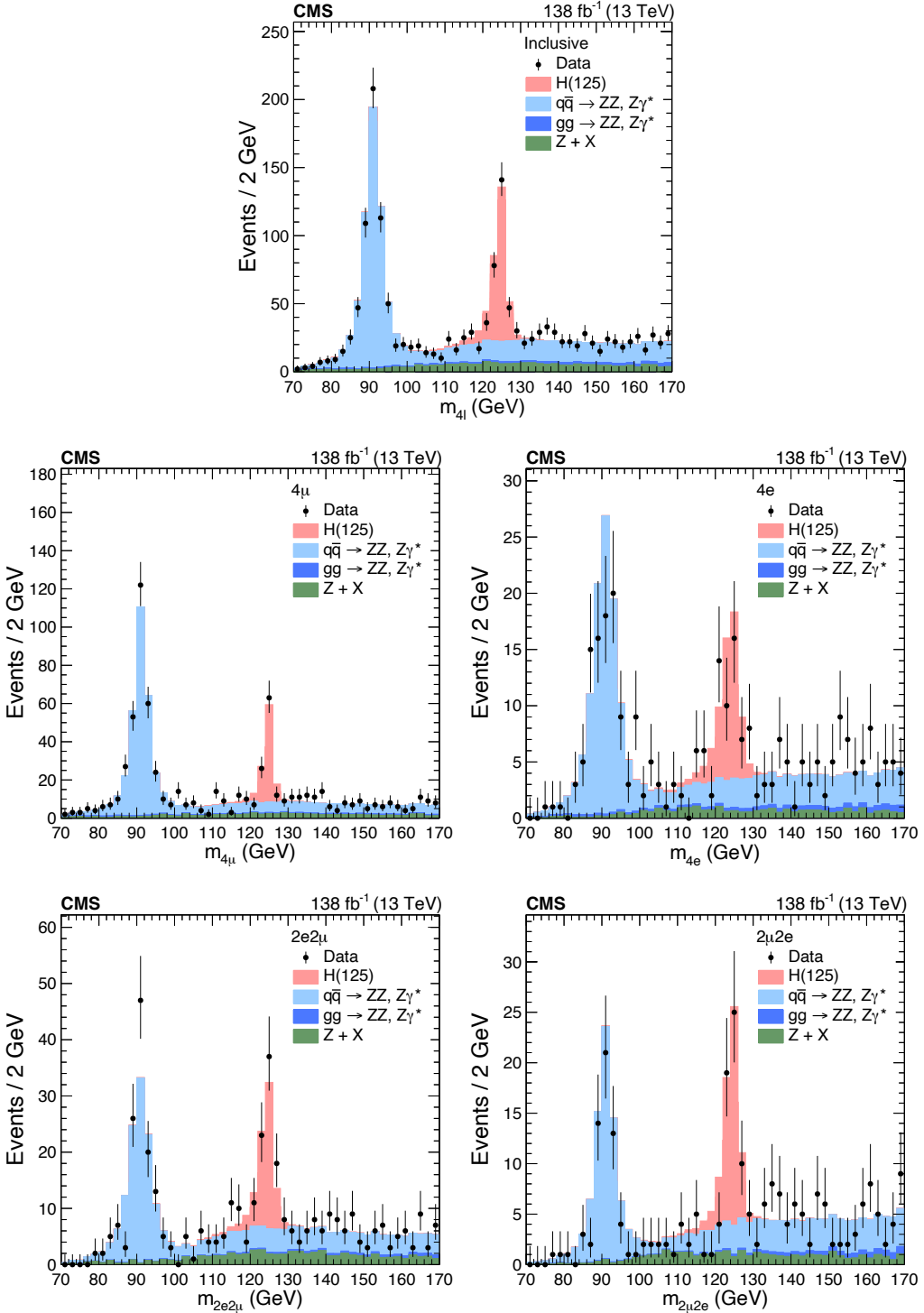


Figure 1: The observed (points) and predicted (stacked histograms) $m_{4\ell}$ distributions in the inclusive (upper), 4μ (middle left), $4e$ (middle right), $2e2\mu$ (lower left) and $2\mu2e$ (lower right) final states, defined such that the first lepton pair is taken to be the one with the mass closest to the nominal Z boson mass. The predictions for the Higgs boson signal and the three main backgrounds are given by the different colors. The vertical bars on the points show the statistical uncertainties in the data.

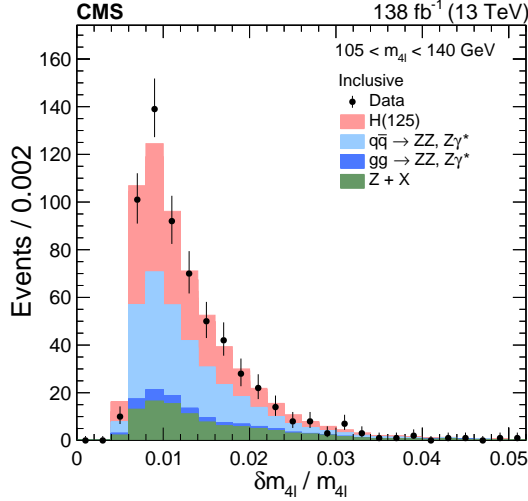


Figure 2: Distributions of the observed (points) and predicted (stacked histograms) relative per-event mass uncertainty of the four-lepton system, in the inclusive final state. The predictions for the Higgs boson signal and the three main backgrounds are given by the different colors. The vertical bars on the points show the statistical uncertainties in the data.

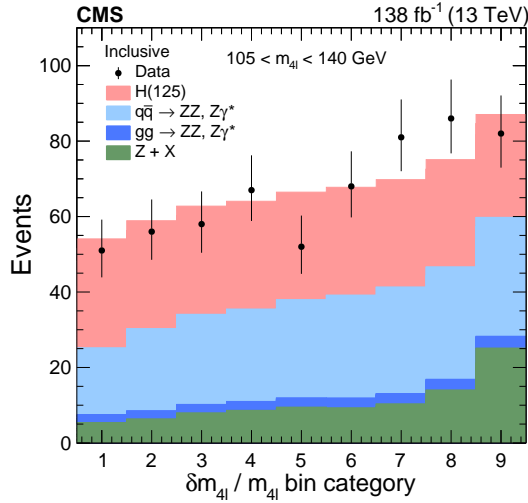


Figure 3: Observed (points) and predicted (stacked histograms) yields of four-lepton events in each of the 9 $\delta m_{4\ell} / m_{4\ell}$ bin categories for the inclusive final state. The bins are shown in the order of increasing $\delta m_{4\ell} / m_{4\ell}$. The predictions for the Higgs boson signal and the three main backgrounds are given by the different colors. The vertical bars on the points show the statistical uncertainties in the data.

and decay processes as

$$\mathcal{D}_{\text{alt}}(\Omega) = \frac{\mathcal{P}_{\text{sig}}(\Omega)}{\mathcal{P}_{\text{sig}}(\Omega) + \mathcal{P}_{\text{alt}}(\Omega)} \quad (3)$$

and

$$\mathcal{D}_{\text{int}}(\Omega) = \frac{\mathcal{P}_{\text{int}}(\Omega)}{2 \sqrt{\mathcal{P}_{\text{sig}}(\Omega) \mathcal{P}_{\text{alt}}(\Omega)}}, \quad (4)$$

where the probability of a certain process \mathcal{P} is calculated using the full set of kinematic observables Ω for the processes denoted as “sig” for a signal model and “alt” for an alternative model,

which can be for either an alternative Higgs boson production mechanism, or a background, depending on the individual case. The “int” label represents the interference between the two model contributions. The probabilities \mathcal{P} are calculated from the matrix elements obtained from the MELA approach.

The $\mathcal{D}_{\text{bkg}}^{\text{kin}}$ discriminant is used in the selection of events, as discussed in Section 4, and as one of the observables in the maximum likelihood fit for the signal extraction, in both the on- and off-shell analyses. It is determined following Eq. (3), where \mathcal{P}_{bkg} is calculated for the dominant $q\bar{q} \rightarrow 4\ell$ background process and \mathcal{P}_{sig} is found for the $H \rightarrow 4\ell$ decay using the full kinematic information of the four leptons. Figure 4 shows the inclusive $\mathcal{D}_{\text{bkg}}^{\text{kin}}$ distribution of the four-lepton system. The inclusion of $\mathcal{D}_{\text{bkg}}^{\text{kin}}$ in the analysis produces a 4% improvement in the $m_{4\ell}$ resolution. In the off-shell analysis, the $\mathcal{D}_{\text{bkg}}^{\text{kin}}$ discriminant is used for events without associated jets.

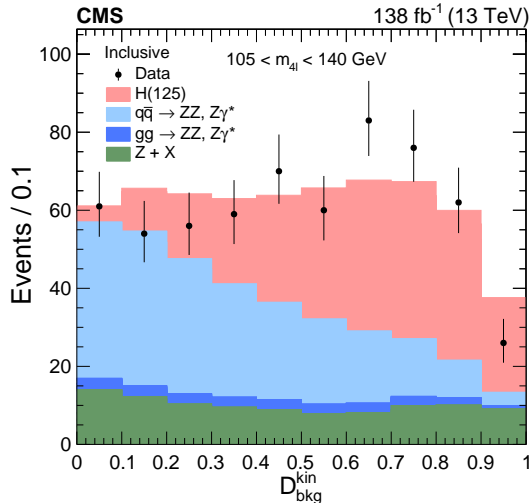


Figure 4: Distributions of the observed (points) and predicted (stacked histograms) $\mathcal{D}_{\text{bkg}}^{\text{kin}}$ of the four-lepton system, in the inclusive final state. The predictions for the Higgs boson signal and the three main backgrounds are given by the different colors. The vertical bars on the points show the statistical uncertainties in the data.

For the two categories of off-shell events with two associated jets described below, VBF- and VH-tagged events, \mathcal{P}_{bkg} and \mathcal{P}_{sig} include the kinematic information on the four leptons and the two jets. The \mathcal{P}_{bkg} probability density corresponds to the EW and QCD background processes with four leptons and two jets, while \mathcal{P}_{sig} is determined for the EW signal processes VBF and VH. Including jet kinematic information in the \mathcal{D}_{bkg} calculation improves the separation of the signal from both the background and ggH production, when compared to $\mathcal{D}_{\text{bkg}}^{\text{kin}}$.

In the analysis of the off-shell region, a dedicated study of a particular kinematic topology is done, treating gluon fusion and EW production separately, because they evolve differently with $m_{4\ell}$, thus allowing us to probe their individual behaviors. Therefore, in the off-shell region, events are further split into three mutually exclusive categories based on the presence of other particles produced in association with the Higgs boson candidate [39]. This is not necessary in the on-shell analysis.

We use various kinematic discriminants and other selection requirements to perform the categorization of the off-shell events. The definition of these discriminants is given by Eq. (3). They are specifically designed to distinguish the targeted signal production mechanisms (VBF, WH,

ZH) within each category from gluon fusion production and are denoted as $\mathcal{D}_{2\text{jet}}^{\text{VBF}}$, $\mathcal{D}_{2\text{jet}}^{\text{ZH}}$, and $\mathcal{D}_{2\text{jet}}^{\text{WH}}$. They are labeled to indicate a specific dijet topology (“2jet”) and production mechanism (VBF, WH, ZH). Calculated using the MELA approach with matrix elements at LO in QCD, these discriminants utilize the complete kinematic information from the Higgs boson decay and the associated jets. Additional details can be found in Refs. [17, 23, 39, 82].

The selected off-shell events are split into three categories: VBF-tagged, VH-tagged, and Untagged events, as summarized in Table 1. The discriminants $\mathcal{D}_{2\text{jet}}$ are constructed following Eq. (3), where \mathcal{P}_{sig} corresponds to the signal probability for VBF (WH or ZH) production in the VBF-tagged (VH-tagged) category, and \mathcal{P}_{alt} to Higgs boson production via ggH in association with two jets. When more than two jets pass the selection criteria, the two jets with the highest p_{T} are chosen for the matrix element calculations. Thereby, the $\mathcal{D}_{2\text{jet}}$ discriminants separate the targeted signal production mode of each category from ggH production using only the kinematic variables of the Higgs boson and the two associated jets. Sequential selection criteria are applied to define the categories as follows:

- The VBF-2jet category requires exactly four leptons. In addition, there must be either two or three jets of which at most one is identified as coming from the hadronization of a b quark, which we term a b-tagged jet [39], or at least four jets and no b-tagged jets. Finally, $\mathcal{D}_{2\text{jet}}^{\text{VBF}} > 0.5$ is required [39].
- The VH-hadronic category requires exactly four leptons. In addition, there must be either two or three jets, or at least four jets and no b-tagged jets. Finally, we demand $\max(\mathcal{D}_{2\text{jet}}^{\text{WH}}, \mathcal{D}_{2\text{jet}}^{\text{ZH}}) > 0.5$ [39].
- The Untagged category consists of the remaining events.

Table 1 provides a summary of the key categorization requirements, with selections applied sequentially from left to right to define the three mutually exclusive categories. All discriminants are calculated with the JHUGEN signal and MCFM background matrix elements. The VH interference discriminant in the VH-tagged category is defined as the simple average of the ones corresponding to the ZH and WH processes. The use of decay kinematic information is denoted by the label “dec”.

Table 1: Summary of the three production categories in the off-shell $m_{4\ell}$ region and the observables used in the fits.

| Category | VBF-tagged | VH-tagged | Untagged |
|-------------|---|---|--|
| Selection | $\mathcal{D}_{2\text{jet}}^{\text{VBF}} > 0.5$ | $\mathcal{D}_{2\text{jet}}^{\text{ZH}} \text{ or } \mathcal{D}_{2\text{jet}}^{\text{WH}} > 0.5$ | Rest of the events |
| Observables | $m_{4\ell}, \mathcal{D}_{\text{bkg}}^{\text{VBF+dec}}, \mathcal{D}_{\text{bsi}}^{\text{VBF+dec}}$ | $m_{4\ell}, \mathcal{D}_{\text{bkg}}^{\text{VH+dec}}, \mathcal{D}_{\text{bsi}}^{\text{VH+dec}}$ | $m_{4\ell}, \mathcal{D}_{\text{bkg}}^{\text{kin}}, \mathcal{D}_{\text{bsi}}^{\text{gg+dec}}$ |

In each category of events, three observables \vec{x} are defined following Eqs. (3) and (4). As summarized in Table 1, $\vec{x} = \{m_{4\ell}, \mathcal{D}_{\text{bkg}}, \mathcal{D}_{\text{int}}\}$. The $m_{4\ell}$ and \mathcal{D}_{bkg} parameters have already been introduced earlier. The third observable, \mathcal{D}_{int} defined in Eq. (4), separates the interference of Higgs boson production (with SM-like couplings) and the background (used as the alternative model). It is called \mathcal{D}_{bsi} for the signal-background interference in the off-shell region. In the Untagged category, decay information is used in the calculation of \mathcal{D}_{int} , as indicated with the label “dec”. In the VBF- and VH-tagged categories, production information from the two associated jets is used, along with decay information. Distributions of the observed and expected \vec{x} observables for events in the off-shell region are illustrated in Fig. 5 for each of the three categories. The expected distributions are found using the SM predicted signal and background cross sections.

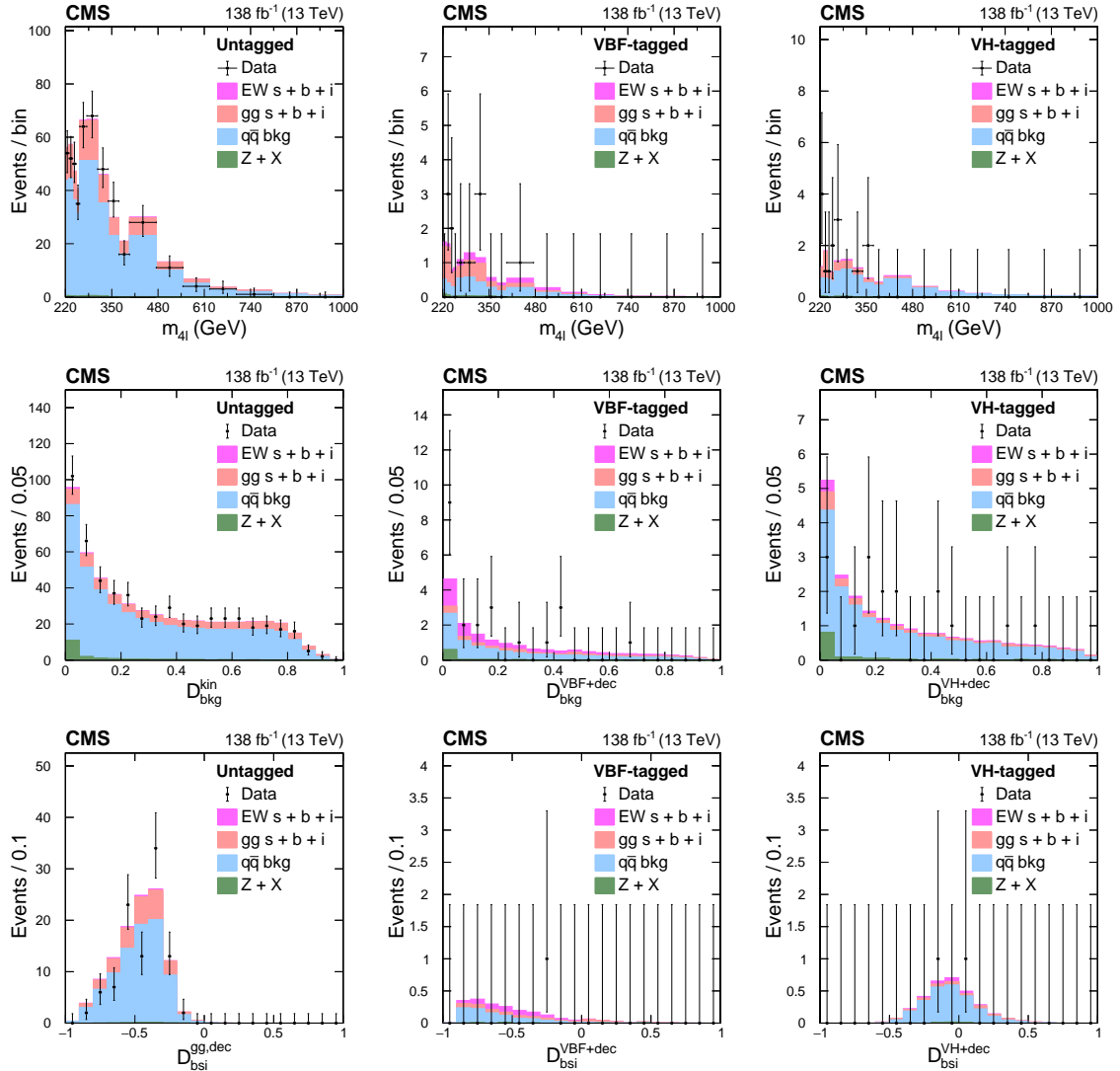


Figure 5: Off-shell data (points) and pre-fit distributions (histograms) for the Untagged (left), VBF-tagged (middle), and VH-tagged (right) categories. The upper row shows $m_{4\ell}$ distributions with a requirement on $D_{\text{bkg}}^{\text{kin}} > 0.6$ (left), $D_{\text{bkg}}^{\text{VBF+dec}} > 0.6$ (middle), or $D_{\text{bkg}}^{\text{VH+dec}} > 0.6$ (right) applied for illustration purposes to enhance signal over background contributions. The middle row shows $D_{\text{bkg}}^{\text{kin}}$ (left), $D_{\text{bkg}}^{\text{VBF+dec}}$ (middle), $D_{\text{bkg}}^{\text{VH+dec}}$ (right) distributions, where an additional requirement $m_{4\ell} > 340 \text{ GeV}$ is applied to enhance signal-over-background contributions. The lower row plots the D_{bsi} with both the $m_{4\ell}$ and $D_{\text{bkg}}^{\text{kin}}$ requirements specified above. Contributions from the four processes are shown by the different colors, where “s”, “b”, and “i” refer to the signal, background, and interference contributions, respectively. The vertical bars on the points give the statistical uncertainties in the data, and the horizontal bars represent the bin widths. For the prefit distributions, the different cross sections are set to their SM values.

7 Estimation of background

The largest background to the Higgs boson signal in the $H \rightarrow 4\ell$ channel is from the process $q\bar{q} \rightarrow ZZ/Z\gamma^*/\gamma^*\gamma^* \rightarrow 4\ell$. The $gg \rightarrow ZZ/Z\gamma^*/\gamma^*\gamma^* \rightarrow 4\ell$ background process, as well as the EW background, which includes the vector boson scattering and VZZ processes, interfere with off-shell Higgs boson production and are discussed in more detail in Sections 3 and 8.

The interference between on-shell Higgs boson production and these backgrounds is, instead, negligible. In the on-shell region, the EW background also incorporates other VVV, $t\bar{t}VV$, and $t\bar{t}V$ processes. To model the $m_{4\ell}$ distributions for each of these irreducible backgrounds, a Bernstein polynomial of third order is used in the $m_{4\ell}$ range 105–140 GeV.

An additional background to the Higgs boson signal, referred to as $Z + X$ in the following, comes from processes in which decays of heavy-flavor hadrons, in-flight decays of light mesons within jets, or charged hadrons overlapping with π^0 decays are misidentified as leptons. The main process contributing to this background is $Z + \text{jets}$ production, which is estimated from control regions in data. The control regions are defined by requiring a lepton pair, satisfying all the requirements of a Z_1 candidate, along with two additional opposite-sign leptons satisfying looser identification requirements than those in the main analysis. These four leptons are then required to pass the Z_1, Z_2 selection. The background yield in the signal region is obtained by weighting the control region events by the lepton misidentification probability (f_ℓ), defined as the fraction of nonsignal leptons that pass the analysis selection criteria. A detailed description of the method can be found in Ref. [17]. The shape of the $m_{4\ell}$ distribution from $Z + X$ events is described by a Landau function. Due to the low number of events, the functional form is extracted using a larger $m_{4\ell}$ range of 70–770 GeV.

The observed number of data events, expected background, and signal yields are listed in Tables 2 and 3 for the on- and off-shell region, respectively. The signal and ZZ background yields are estimated from simulation, while the $Z + X$ yield is estimated from data. The details of the Higgs boson signal modeling, its interference with background, and the ZH cross-feed for the off-shell results are given in Section 8.

Table 2: The observed and expected yields for the Higgs boson signal and background contributions in the on-shell region $105 < m_{4\ell} < 140$ GeV, for each of the four-lepton categories and the total.

| | 4μ | $4e$ | $2e2\mu$ | $2\mu2e$ | Total |
|---|--------|-------|----------|----------|-------|
| Total signal | 90.9 | 48.7 | 65.5 | 53.3 | 258.4 |
| $q\bar{q} \rightarrow 4\ell$ background | 89.2 | 38.9 | 64.4 | 42.1 | 234.6 |
| $gg \rightarrow 4\ell$ background | 9.7 | 4.9 | 4.9 | 3.8 | 23.4 |
| $Z + X$ background | 32.4 | 12.2 | 28.2 | 18.6 | 91.3 |
| Total expected | 222.2 | 104.6 | 163.0 | 117.8 | 607.7 |
| Observed | 230 | 94 | 170 | 107 | 601 |

8 Extraction of signal

The modeling of the signal process is different for the on- and off-shell regions. In the on-shell region, there is negligible interference between the Higgs boson and background production, so the signal can be treated separately. At the same time, the narrow Higgs boson peak requires careful treatment of the detector resolution effects. There is also little dependence on the production processes because the $H \rightarrow 4\ell$ decay is independent of the production mechanism due to the narrow-width approximation. In the off-shell region, on the other hand, the distributions are much wider, with minimal influence from detector resolution on the measurements. However, there is a sizable interference between the Higgs boson signal and background processes, and their proper treatment requires special care. Moreover, the treatment of the gluon fusion and EW productions is different because of their different evolution with $m_{4\ell}$.

Table 3: Observed and expected yields for the Higgs boson signal and background contributions in the off-shell region $m_{4\ell} > 220 \text{ GeV}$, for each of the four-lepton categories and the total. The yields from interference of the signal and background and the ZH cross-feed are also shown.

| | VBF-tagged | VH-tagged | Untagged | Total |
|--|------------|-----------|----------|--------|
| gg $\rightarrow 4\ell$ signal | 1.0 | 0.9 | 25.1 | 27.0 |
| gg $\rightarrow 4\ell$ background | 16.0 | 13.5 | 457.0 | 486.4 |
| gg $\rightarrow 4\ell$ interference | -2.1 | -1.9 | -52.0 | -56.1 |
| EW signal | 1.3 | 0.1 | 1.8 | 3.2 |
| EW background | 14.9 | 2.9 | 19.7 | 37.5 |
| EW interference | -3.4 | -0.2 | -3.9 | -7.4 |
| ZH cross-feed | 0.2 | 0.4 | 7.0 | 7.6 |
| q \bar{q} $\rightarrow 4\ell$ background | 28.6 | 46.7 | 1795.1 | 1870.4 |
| Z + X background | 4.7 | 5.3 | 89.7 | 99.7 |
| Total expected | 61.2 | 67.8 | 2339.4 | 2468.4 |
| Observed | 70 | 67 | 2335 | 2472 |

8.1 Signal modeling in the on-shell region

The probability density for the on-shell region includes both signal and background contributions. It is normalized to the total event yield for each process j and category k , and can be written as

$$\mathcal{P}_{jk}(\vec{x}; \vec{\xi}_{jk}, \vec{\zeta}) = \mu_j \mathcal{P}_{jk}^{\text{sig}}(\vec{x}; \vec{\xi}_{jk}, \vec{\zeta}) + \mathcal{P}_{jk}^{\text{bkg}}(\vec{x}; \vec{\xi}_{jk}), \quad (5)$$

where $\vec{\zeta}$ are the unconstrained parameters of interest, including the signal strength μ_j defined as the ratio of the signal yield to the SM expectation, $\vec{\xi}_{jk}$ are the constrained nuisance parameters for a particular parametrization, and \vec{x} are the observables.

In the on-shell Higgs boson mass and width analysis, there are six signal processes (ggH, VBF, VH, t \bar{t} H, b \bar{b} H, and tqH) and three background processes (q \bar{q} /gg $\rightarrow ZZ/Z\gamma^*/\gamma^*\gamma^* \rightarrow 4\ell$ and Z + X). When constraints on Γ_H are determined by simultaneously fitting both the on-shell and off-shell regions, the on-shell region follows Scheme 2 as described in Ref. [83], where additional details on categorization and signal and background modeling can be found. Additional details regarding the signal modeling for the mass and width analyses using only the on-shell region are provided below.

For the Higgs boson mass measurement, a one-dimensional (1D) statistical model is built in each category using the observable $m_{4\ell}$, split between data-taking years and final states, and taking each of the nine $\delta m_{4\ell} / m_{4\ell}$ bins separately. The signal shape for each process is obtained from a fit of the simulated $m_{4\ell}$ distribution, in the range 105–140 GeV, using a double-sided Crystal Ball function [84]. In the case of VH and t \bar{t} H production, a Landau function is added to include the possible contribution of a lepton from Higgs boson decay being outside the detector acceptance or failing the selection criteria. Five simulated mass points (120, 124, 125, 126, and 130 GeV) are used to parametrize the m_H dependence of each shape parameter p^i in the Crystal Ball and Landau functions. A set of first-order polynomials with constants a^i and b^i is fitted simultaneously as functions of m_H :

$$p^i = a^i + b^i(m_H - 125 \text{ GeV}). \quad (6)$$

The natural width of the Higgs boson is assumed to be much smaller than the instrumental $m_{4\ell}$ resolution. For the on-shell width measurement instead, the signal shape is the convolution

of a Crystal Ball function with a Breit–Wigner function, to include Γ_H as a parameter in the model. This model is referred to as 1D. If the BS and $m(Z_1)$ constraints are applied, the model is referred to as $1D'_{BS}$. Figure 6 shows an example of the signal model used in the on-shell analysis and how it varies across the $\delta m_{4\ell} / m_{4\ell}$ bins. This categorization isolates the events

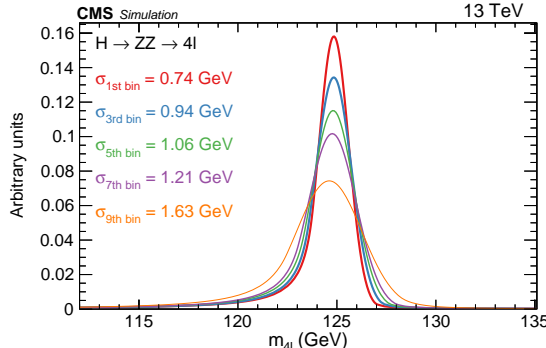


Figure 6: Examples of the on-shell signal model $m_{4\ell}$ shape for five $\delta m_{4\ell} / m_{4\ell}$ bins. For illustration purposes, the mass range shown is reduced to 112–135 GeV, and all final states and all data-taking years are combined. The resolution estimator $\sigma_{i \text{ bin}}$ is defined as the width of the Gaussian function from a fit to events in bin i having the smallest mass window that contains 68% of the signal events.

with better invariant mass resolution and improves the description of the signal shape and the modeling of the peak position. This latter improvement is most important for the final state where the on-shell Z boson decays to two electrons. An illustration of the full model used in the on-shell analysis is shown in Fig. 7.

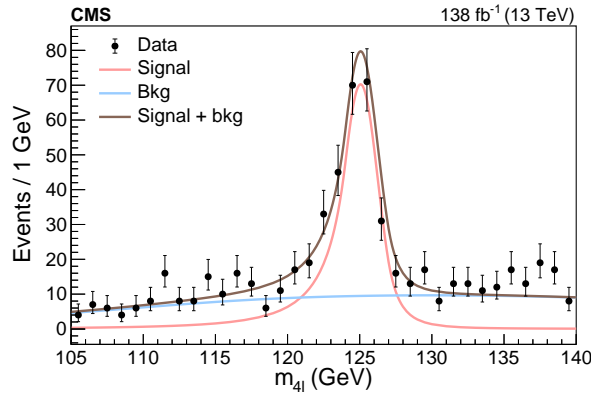


Figure 7: Illustration of how the on-shell statistical model is constructed, combining the $m_{4\ell}$ distributions from all data-taking years and all final states. The red, blue, and brown lines show the results of the fit to the signal, background, and their sum, respectively.. The solid black points with vertical bars show the data and the associated statistical uncertainties.

Based on the 1D model, a two-dimensional (2D) statistical model is built with a probability density \mathcal{P}_{2D} using the observables $m_{4\ell}$ and \mathcal{D}_{bkg}^{kin} and the expression

$$\mathcal{P}_{2D}(m_{4\ell}, \mathcal{D}_{bkg}^{kin}) = \mathcal{P}_{1D}^{\text{sig}} T^{\text{sig}}(\mathcal{D}_{bkg}^{kin} | m_{4\ell}) + \mathcal{P}_{1D}^{\text{bkg}} T^{\text{bkg}}(\mathcal{D}_{bkg}^{kin} | m_{4\ell}).$$

The factor T , based on a 2D histogram template, is a conditional probability density function of \mathcal{D}_{bkg}^{kin} and $m_{4\ell}$, implemented by normalizing the sum of the contents in each $m_{4\ell}$ histogram bin to one.

The final model, designated \mathcal{N} -2D is built by combining all 2D models of \mathcal{N} different $\delta m_{4\ell} / m_{4\ell}$ categories. If the BS and $m(Z_1)$ constraint approaches are applied, the model is referred to as \mathcal{N} -2D_{BS}'. This configuration provides the best Higgs boson mass and width precision and is used as the default for the on-shell measurements. A simultaneous signal-plus-background unbinned fit to all categories is performed to extract m_H and Γ_H . The signal strength is left unconstrained in this fit.

8.2 Signal and background interference modeling in the off-shell region

In the off-shell region, the probability density follows Eqs. (1) and (5) closely, with the additional contribution of the interference (“int”) between the signal and background amplitudes, as well as a cross-feed (“cross”) component discussed below. It is parametrized as

$$\mathcal{P}_{jk}(\vec{x}; \vec{\xi}_{jk}, \vec{\zeta}) = \frac{\mu_j \Gamma_H}{\Gamma_0} \mathcal{P}_{jk}^{\text{sig}}(\vec{x}; \vec{\xi}_{jk}) + \sqrt{\frac{\mu_j \Gamma_H}{\Gamma_0}} \mathcal{P}_{jk}^{\text{int}}(\vec{x}; \vec{\xi}_{jk}) + \mu_j \mathcal{P}_{jk}^{\text{cross}}(\vec{x}; \vec{\xi}_{jk}) + \mathcal{P}_{jk}^{\text{bkg}}(\vec{x}; \vec{\xi}_{jk}), \quad (7)$$

where Γ_0 is the reference value of the Higgs boson width (not necessarily its SM value) used in simulation. Otherwise, the definition of the terms is the same as in Eq. (5). In the off-shell width analysis, there are two production modes, j (gluon fusion and EW, which includes both VBF and VH), and three jet-tagged categories, k . All lepton flavors and data periods are combined in this analysis. The contributions from $t\bar{t}H$, $b\bar{b}H$, and tqH are expected to be negligible in the off-shell region.

The $\mathcal{P}_{jk}^{\text{sig}}$, $\mathcal{P}_{jk}^{\text{int}}$, $\mathcal{P}_{jk}^{\text{cross}}$, and $\mathcal{P}_{jk}^{\text{bkg}}$ probability densities are normalized to the expected number of events, and are implemented as binned histograms (templates) of the observables \vec{x} listed in Table 1. These templates are obtained as weighted linear combinations of existing simulated signal or background samples.

The off-shell region includes all events with $m_{4\ell}$ greater than 220 GeV. Other processes can mimic off-shell Higgs boson production and decay to four leptons in this region. Specifically, we study on-shell signal events in which the Higgs boson decays to $2\ell + X$, and X contains further leptons that allow the event to pass the four-lepton selections. The dominant on-shell Higgs boson process that can contaminate the off-shell region is $Z(\ell\ell)H(2\ell + X)$, called ZH cross-feed.

The ZH cross-feed contribution is estimated using on-shell ZH samples with $H \rightarrow WW$ and ZZ decays, where both hadronic and leptonic decay of the Z bosons is allowed. The dominant contributions come from the $H \rightarrow 2\ell 2\nu$ and $2\ell 2q$ final states produced in association with $Z \rightarrow 2\ell$. To prevent double counting, on-shell cross-feed events are eliminated from the off-shell simulated samples.

The gluon fusion cross section is calculated using the highest order QCD and EW expansions available to simulate inclusive ZZ production [13]. However, event categorization depends on modeling associated jets through PYTHIA’s parton showering and hadronization, which involves matching these processes to the hard-scattering production. Off-shell gluon fusion production is generated at LO with no associated jets at the matrix element level, and therefore all jets come from PYTHIA. The parton showering and hadronization requires setting the hadronization scale, which can depend on the energy scale in the process. In the case of the $gg \rightarrow 4\ell$ process, the energy scale is set at $m_{4\ell}$.

The EW cross section for the inclusive production of ZZ and two associated jets is also calculated to the highest order QCD and EW expansion available [13]. Contrary to the gluon fusion

process, two hard jets, which are typically the leading jets in the process, are already generated at the matrix element level in the LO simulation. These are the two associated jets in the VBF process, or the two jets from the hadronic decay of the associated W or Z boson. Therefore, the dependence on the PYTHIA parton shower and hadronization and its matching to the hard-scattering production is much weaker for these EW processes.

The categorization efficiency of simulated ggH and EW Higgs boson production can be checked using alternative POWHEG and MINLO simulations. The POWHEG samples are generated for a wide range of off-shell Higgs boson masses at NLO in QCD, with one jet generated at the matrix element, and using PYTHIA matching to simulate additional jets. The MINLO simulation of ggH production is done for Higgs boson masses of 125 and 300 GeV at NLO in QCD, with two jets generated at the matrix element level, and PYTHIA matching for additional jets. While the JHUGEN categorization efficiencies agree with those using POWHEG and MINLO within the uncertainties of the QCD scale used in PYTHIA, for the ggH process the deviations of the central values and the corresponding uncertainties are up to 20% in the signal-dominated $m_{4\ell}$ range 300–500 GeV, depending on the category. In the EW process, categorization efficiencies from the two approaches typically agree within 5–10%. In all cases, we adjust the categorization efficiency as a function of $m_{4\ell}$ to match that for the SM signal obtained from the POWHEG samples, and assume the same behavior for the background and interference contributions. This correction procedure ensures that the total event yield, summed over the three categories, is unchanged at each value of $m_{4\ell}$.

Simulation of the \vec{x} observables listed in Table 1 is not affected by the jet modeling in the Untagged category. It is also found that the modeling of the observables in the jet-tagged categories is nearly the same in the EW process, when compared between the direct MCFM + JHUGEN samples and reweighted POWHEG + JHUGEN. However, the modeling of jets in the jet-tagged categories for the ggH process does impact the parametrization of the probability distributions. Therefore, within these two jet-tagged categories, the gluon fusion process is incorporated through the reweighted POWHEG + JHUGEN simulation. This approach allows a more precise matching with the parton shower, thereby better describing the associated jet activity. In this case, the samples are reweighted for the appropriate model using the MELA package, as discussed in Section 3.

9 Systematic uncertainties

Several systematic uncertainties are estimated in the measurement of the constrained parameters $\tilde{\zeta}_{jk}$. The template shapes describing the probability distributions in Eqs. (5) and (7) are varied separately within either the theoretical or experimental uncertainties, and the resulting variation in the constrained parameters is taken as the systematic uncertainty from this source.

The largest systematic uncertainties in the on-shell determination of the Higgs boson mass and width are in the lepton momentum scale and resolution. The estimation of the scale uncertainty is extracted in a two-step process. First, the offsets in the measured Z boson mass peak position with respect to the nominal Z boson mass in data and simulation are extracted, as a function of p_T and $|\eta|$ of the related leptons. The estimate of this effect is about 0.02 and 0.12% for muons and electrons, respectively, independent of the data-taking year. In the second step, the systematic uncertainties affecting the corrections are propagated to the $m_{4\ell}$ distribution. Considering both effects, the estimated systematic uncertainties are 0.03 and 0.15% in the muon and electron momentum scales, respectively, with an uncertainty in the corresponding Higgs boson invariant mass resolutions of 3 and 10%.

The largest systematic uncertainty in the off-shell measurement of the Higgs boson width is from the modeling of the dominant background process $q\bar{q} \rightarrow ZZ/Z\gamma^*/\gamma^*\gamma^* \rightarrow 4\ell$. Experimental uncertainties specific to the off-shell analysis involve those from the jet energy calibration, which are only relevant for the VBF- and VH-tagged categories.

Theoretical uncertainties that affect both the signal and background estimations include those from the renormalization and factorization scales, and the choice of the parton distribution function set. The uncertainty from the renormalization and factorization scales is determined by varying these scales by factors of 0.5 and 2 from their nominal values while keeping the ratio of the two scales between 0.5 and 2. The uncertainty due to the parton distribution function set is estimated by taking the root mean square of the variations when using different replicas of the default NNPDF set. An additional uncertainty of 10% in the K factor used for the $gg \rightarrow ZZ$ prediction is applied.

The integrated luminosities for the 2016, 2017, and 2018 data-taking years have 1.2–2.5% individual systematic uncertainties [85–87], while the overall uncertainty for the 2016–2018 period is 1.6%. The uncertainty in the lepton identification, reconstruction, and selection efficiency ranges from 2 to 14% in terms of the overall event yield for the 4μ and $4e$ final states, respectively, and affects both signal and background processes.

In the estimation of the $Z + X$ background, the flavor composition of hadronic jets misidentified as leptons can be different in the $Z + 1\ell$ and $Z + 2\ell$ control regions. Together with the statistical uncertainty in the $Z + 2\ell$ region, this uncertainty accounts for about a 30% variation in the background yields. The uncertainty in the modeling of this misidentification rate as a function of p_T and η , combined with the $Z + 1\ell$ control region statistical uncertainty, leads to uncertainties in the backgrounds yields ranging from 32% in the $4e$ final state to 39% in the 4μ .

10 Higgs boson mass and width measurements with on-shell production

The Higgs boson mass is measured using different likelihood models as described in Section 8.1. Table 4 shows the mass measurements obtained from the 1D approach, where no further assumptions have been made. In comparison to the 1D model, the $1D'_{BS}$ model (as described in Section 5) reduces the uncertainty by about 15%. Implementing the $\delta m_{4\ell}/m_{4\ell}$ categorization then gives the $\mathcal{N}-1D'_{BS}$ model, which leads to an additional 10% improvement. Finally, using the D_{bkg}^{kin} discriminant to reduce the background produces the $\mathcal{N}-2D'_{BS}$ model with another 4% improvement. Table 5 shows the resulting $m_{4\ell}$ measurements using this last model. All the measured $m_{4\ell}$ values from the different fits are statistically compatible, given their uncertainties and correlations. Figure 8 displays the observed 1D likelihood scans as functions of m_H , from the fits for the different 4ℓ categories and combined. Combining all the $m_{4\ell}$ final states and data-taking years, our final result is $m_H = 125.04 \pm 0.11 \text{ (stat)} \pm 0.05 \text{ (syst)} = 125.04 \pm 0.12 \text{ GeV}$. The largest systematic uncertainty is from the lepton momentum scale and equals 0.03 and 0.04 GeV for final states with muons and electrons, respectively.

As a check on the analysis technique and the systematic uncertainty from this method, the $1D'_{BS}$ model is applied to $Z \rightarrow 4\ell$ events in the $m_{4\ell}$ range 70–105 GeV. The signal shape is obtained using a convolution of a Breit–Wigner function and a double-sided Crystal Ball function. The fitted values of m_Z in different subchannels are $m_Z^{4\mu} = 91.02 \pm 0.14 \text{ GeV}$, $m_Z^{4e} = 91.18 \pm 0.45 \text{ GeV}$, $m_Z^{2e2\mu} = 91.40 \pm 0.29 \text{ GeV}$, and $m_Z^{2\mu2e} = 91.40 \pm 0.37 \text{ GeV}$, leading to a combined value of $m_Z = 91.17 \pm 0.12 \text{ GeV}$, consistent with the world-average Z boson mass [89]

Table 4: Best fit values for the mass of the Higgs boson measured in the inclusive 4ℓ final state and separately for different flavor categories using the 1D approach. Uncertainties are separated into statistical and systematic uncertainties. Expected uncertainties are also given assuming $m_H = 125.38 \text{ GeV}$ [88].

| 4ℓ category | Observed ($\pm \text{stat} \pm \text{syst}$) (GeV) | Expected uncertainty ($\pm \text{stat} \pm \text{syst}$) (GeV) |
|------------------|--|--|
| Inclusive | $124.98 \pm 0.14 \pm 0.05$ | $\pm 0.14 \pm 0.05$ |
| 4μ | $124.87 \pm 0.17 \pm 0.04$ | $\pm 0.18 \pm 0.04$ |
| $2\mu 2e$ | $125.32^{+0.36}_{-0.37} \pm 0.10$ | $+0.34+0.09$ $-0.34-0.10$ |
| $2e 2\mu$ | $125.23^{+0.36+0.09}_{-0.35-0.11}$ | $+0.35+0.09$ $-0.35-0.10$ |
| $4e$ | $124.94^{+0.68}_{-0.71} \pm 0.20$ | $+0.51+0.18$ $-0.51-0.20$ |

Table 5: Best fit values for the mass of the Higgs boson measured in the inclusive 4ℓ final state and separately for different flavor categories, using the final fit configuration ($\mathcal{N}\text{-}2\text{D}'_{BS}$). Uncertainties are separated into statistical and systematic uncertainties. Expected uncertainties are also given assuming $m_H = 125.38 \text{ GeV}$ [88].

| 4ℓ category | Observed ($\pm \text{stat} \pm \text{syst}$) (GeV) | Expected uncertainty ($\pm \text{stat} \pm \text{syst}$) (GeV) |
|------------------|--|--|
| Inclusive | $125.04 \pm 0.11 \pm 0.05$ | $\pm 0.11 \pm 0.05$ |
| 4μ | $124.90 \pm 0.14 \pm 0.05$ | $\pm 0.14 \pm 0.04$ |
| $2e 2\mu$ | $125.50^{+0.25}_{-0.24} \pm 0.10$ | $\pm 0.24 \pm 0.10$ |
| $2\mu 2e$ | $125.20^{+0.27+0.11}_{-0.26-0.07}$ | $\pm 0.27 \pm 0.10$ |
| $4e$ | $124.70^{+0.49}_{-0.47} \pm 0.20$ | $\pm 0.38 \pm 0.20$ |

and with the uncertainty in agreement with the expected value of $\pm 0.12 \text{ GeV}$ from simulation.

10.1 Higgs boson mass measurement with Runs 1 and 2 data combined

The results from this analysis are combined with those extracted using data recorded with the CMS detector during Run 1 at $\sqrt{s} = 7$ and 8 TeV [90]. Since this analysis uses an improved method to extract the systematic uncertainties affecting lepton momentum, the lepton energy scales and resolution uncertainties are considered uncorrelated between the two runs. The combined observed result from both data-taking periods is $m_H = 125.08 \pm 0.12 \text{ GeV} = 125.08 \pm 0.10 \text{ (stat)} \pm 0.05 \text{ (syst)} \text{ GeV}$. The corresponding expected statistical and systematic uncertainties are ± 0.10 and $\pm 0.05 \text{ GeV}$, respectively. Figure 9 presents a summary of the Higgs boson mass measurements by the CMS Collaboration in the four-lepton decay channel.

10.2 Higgs boson width measurement from on-shell production

The Higgs boson width is measured using on-shell production by fitting the $m_{4\ell}$ distribution in the mass range $105 < m_{4\ell} < 140 \text{ GeV}$. The $\mathcal{N}\text{-}2\text{D}'_{BS}$ model used for the mass measurement is adopted also in this case, changing the signal model, as described before, to include the Γ_H parameter. Since the theoretical value is very close to zero, which is a strict lower bound,

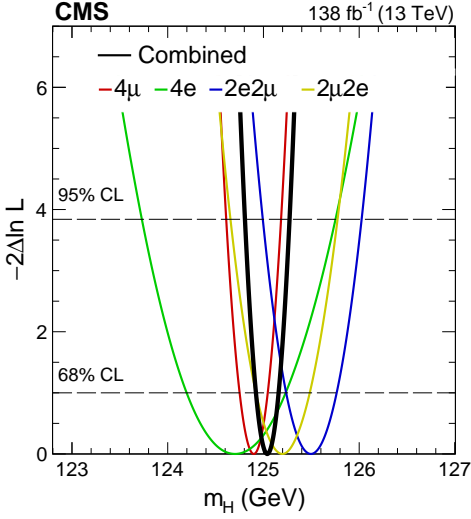


Figure 8: The profile likelihood from the m_H fit using the $\mathcal{N}-2D'_{BS}$ model for each of the 4ℓ categories and combined. The change in likelihood corresponding to 68 and 95% CLs are shown by the dashed horizontal lines. Both statistical and systematic uncertainties are included in the fits.

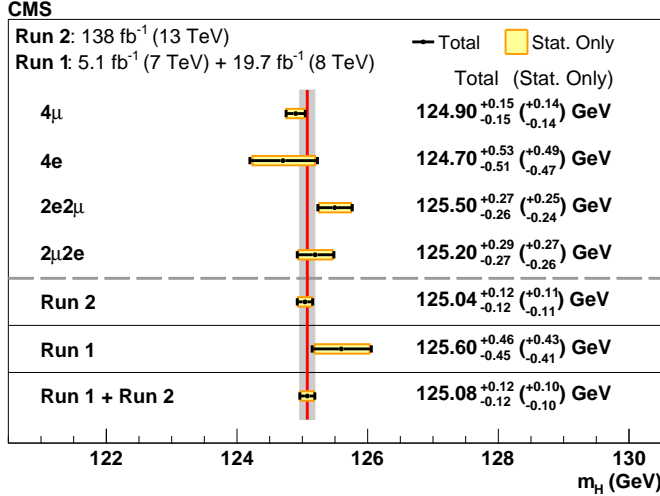


Figure 9: Summary of the CMS Higgs boson mass measurements using the four-lepton final state. The red vertical line and the gray column represent the best fit value and the total uncertainty, respectively, as measured by combining the Runs 1 and 2 data. The yellow band and horizontal black bars show the statistical and total uncertainties in each measurement, respectively. The value of each measurement is given, along with the total and statistical only (in parentheses) uncertainties.

confidence intervals for the Higgs boson width are obtained following the Feldman–Cousins approach [91]. The CL is evaluated for several width hypotheses using distributions obtained from simulated pseudo-experiments. In this process, the nuisance parameters are fixed to their best fit values. The observed (expected) upper limit on Γ_H is 50 (320) MeV at 68% CL and 330 (640) MeV at 95% CL. Although the observed limit is much less than the expected one, the two are statistically compatible. The resulting distribution of $1 - \text{CL}$ vs. Γ_H is shown in Fig. 10.

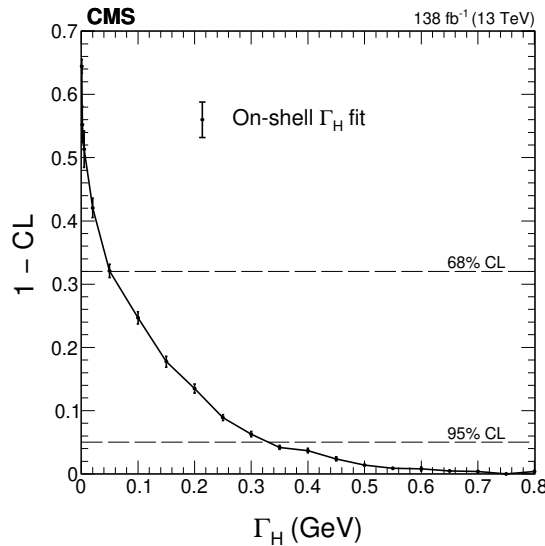


Figure 10: Distribution of $1 - CL$ vs. Γ_H from the fit in the measurement of the Higgs boson width using on-shell production only. The CL values shown by the points are extracted using the Feldman-Cousins approach. The vertical bars on the points represent the spread of the simulated pseudo-experiment values. The 68 and 95% CL values are shown by the dashed horizontal lines.

11 Higgs boson width measurement with off-shell production

We perform an extended binned maximum likelihood fit to the on- and off-shell events split in several categories. The final measurements on m_H , Γ_H , and μ_j are conducted using the profile likelihood method [92] implemented in the ROOFIT toolkit [93] within the ROOT [94] framework. The extended likelihood function is constructed using the probability densities in Eqs. (5) and (7), with each event characterized by the discrete category k and typically three observables \vec{x} . The likelihood \mathcal{L} is maximized with respect to the nuisance parameters $\vec{\zeta}_{jk}$ describing the systematic uncertainties and the signal strength parameters μ (total signal strength), or μ_F (signal strength for ggH) and μ_V (signal strength for the EW processes). The allowed 68 and 95%CL intervals are defined using the profile likelihood function, $-2\Delta \ln \mathcal{L} = 1.00$ and 3.84 , respectively, for which exact coverage is expected in the asymptotic limit [95].

Constraints on Γ_H are set by simultaneously fitting $H \rightarrow ZZ \rightarrow 4\ell$ events from the on- and off-shell regions. The on-shell region corresponds to Scheme 2 in Ref. [83], where six mutually exclusive event categories are defined and anomalous interactions are constrained to zero. It determines the signal strengths $\mu_F^{\text{on-shell}}$ and $\mu_V^{\text{on-shell}}$, corresponding to production mechanisms driven by fermion and vector boson couplings of the Higgs boson, respectively, as defined in Section 1. The Higgs boson mass is constrained to $m_H = 125.38$ GeV [88] in this fit. In the on- and off-shell parametrizations in Eqs. (5) and (7), we set $\mu_F^{\text{on-shell}} = \mu_F^{\text{off-shell}}$ and $\mu_V^{\text{on-shell}} = \mu_V^{\text{off-shell}}$. The observed and expected constraints on the Higgs boson width are shown in Table 6. The likelihood scan of Γ_H using the asymptotic approximation method is shown in Fig. 11. This measurement excludes the scenario of no off-shell Higgs boson production with a CL corresponding to 3.0 standard deviations (average expected 1.4).

The observed limits on Γ_H are stronger than the average expected values from simulation. This is supported by the upper left plot of Fig. 5, where the number of observed events in the sensitive region of $m_{4\ell} > 340$ GeV and $\mathcal{D}_{\text{bkg}} > 0.6$ in the Untagged category is below the ex-

Table 6: Summary of the total Higgs boson width Γ_H measurement, showing the 68% CL (central values with uncertainties) and 95% CL (in square brackets) intervals for the $H \rightarrow ZZ \rightarrow 4\ell$ channel alone and in combination with the off-shell $H \rightarrow ZZ \rightarrow 2\ell 2\nu$ channel.

| Channel | Observed Γ_H (MeV) | Expected Γ_H (MeV) |
|--|--------------------------------|----------------------------|
| 4 ℓ on- and off-shell | $2.9^{+2.3}_{-1.7}$ [0.3, 7.9] | 4.1 ± 4.0 [< 11.5] |
| 4 ℓ on- and off-shell + 2 $\ell 2\nu$ off-shell | $3.0^{+2.0}_{-1.5}$ [0.6, 7.3] | 4.1 ± 3.5 [0.1, 10.5] |

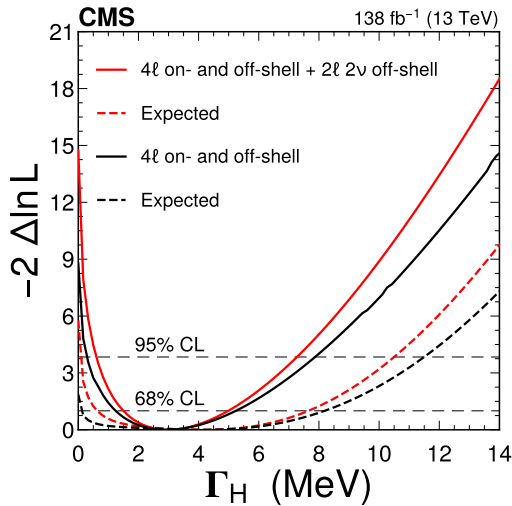


Figure 11: Observed (solid) and expected (dashed) profile likelihood projections from the Higgs boson width fit using on- and off-shell production from this analysis. The analysis of the off-shell $H \rightarrow ZZ \rightarrow 4\ell$ channel combined with the on-shell $H \rightarrow ZZ \rightarrow 4\ell$ channel [83] is shown in black. The full combination of $H \rightarrow ZZ \rightarrow 4\ell$ with the off-shell $H \rightarrow ZZ \rightarrow 2\ell 2\nu$ [24] is given in red. The black horizontal dashed lines show the 68 and 95% CL values.

pected value, but still consistent with it. The smaller number of events in this region favors the hypothesis of negative interference between the signal and background contributions, which dominates over the pure signal contributions for Γ_H values near the SM value. Therefore, large and very small values of Γ_H are disfavored.

11.1 Examination of model dependency in width measurement

The above Γ_H constraints assume the expected SM-like evolution of the Higgs boson couplings over a large $m_{4\ell}$ range. The anomalous contributions to the HVV vertex in EW production and Higgs boson decay were evaluated in our earlier analyses using a smaller data set [23, 24], and the constraints on Γ_H remained consistent. However, the predominance of the top quark in the ggH loop is assumed here and in our previous analyses. If there are additional contributions, such as from yet undiscovered heavy particles, then the $m_{4\ell}$ evolution in the off-shell region would be altered.

To investigate the impact of large-mass yet undiscovered particles in the ggH loop, we introduce a new heavy quark Q with an unconstrained coupling strength κ_Q in the likelihood parametrization, as described in Refs. [52, 96]. In the framework of effective field theories, the contribution of Q can be interpreted as a point-like interaction that encapsulates the influence of any heavy particles present in the loop. The parameterization in Eq. (7) is extended to include the templates for terms proportional to κ_Q^2 and κ_Q , utilizing simulations reweighted with

the MELA package in the limit of the infinite Q mass. The $m_{4\ell}$ shape in the off-shell region shows contrasting patterns between the SM ggH production, which is mainly affected by the top quark loop with the $2m_t$ threshold effect, and the Higgs boson produced via ggH loop involving the heavy quark Q [52].

An unconstrained κ_Q introduces additional uncertainty into the $m_{4\ell}$ dependence in the off-shell region, resulting in less stringent limits on Γ_H . However, both on- and off-shell $H \rightarrow 4\ell$ data constrain the possible values of κ_Q , and the constraints on Γ_H remain largely consistent with those for $\kappa_Q = 0$. The resulting Γ_H measurement from the combined on- and off-shell events is $2.7^{+2.7}_{-1.8}$ MeV (expected $4.1^{+5.3}_{-4.0}$ MeV). The observed (expected) 95% CL interval is $[0.1, 8.7]$ ($[<14.1]$) MeV. We note that combining measurements from other on-shell Higgs boson production and decay channels in the future will lead to much stricter constraints on κ_Q , reducing the flexibility to alter the SM-like evolution of the Higgs boson couplings over a large $m_{4\ell}$ range.

11.2 Higgs boson width measurement with a combination of off-shell channels

The results of this analysis with the SM-like couplings are combined with the prior CMS off-shell $H \rightarrow ZZ \rightarrow 2\ell 2\nu$ analysis [24], giving the first CMS measurement of Γ_H using the full 4ℓ and $2\ell 2\nu$ data sample collected during Run 2. The observed and expected Γ_H measurements are shown in Table 6 and Fig. 11 and supersede the previous CMS results [24] under the SM-like coupling assumption. The fit results rule out the scenario of no off-shell Higgs boson production with a CL corresponding to 3.8 standard deviations (average expected 2.4).

The off-shell region fit can also be performed without relating its signal strength to that for the on-shell region. In this case, the signal strength is modified by the parameter $\mu^{\text{off-shell}}$ common to all production mechanisms, with $\Gamma_H = \Gamma_H^{\text{SM}}$ in Eq. (7), and the SM expectation corresponding to $\mu^{\text{off-shell}} = 1$. In addition, we also perform a fit of the off-shell events with two unconstrained parameters $\mu_F^{\text{off-shell}}$ and $\mu_V^{\text{off-shell}}$, which express the signal strengths in the ggH and EW processes, respectively. The measured signal strengths are reported in Table 7 and a 2D scan of these parameters is presented in Fig. 12. The observed limits on signal strength in the off-shell region are stronger than expected on average, following a trend similar to that previously discussed for Γ_H .

Table 7: Measured values of the signal strengths $\mu^{\text{off-shell}}$, $\mu_F^{\text{off-shell}}$, and $\mu_V^{\text{off-shell}}$, and their 68% and 95% (in square brackets) CL intervals from the combined fit to the off-shell $H \rightarrow ZZ \rightarrow 4\ell$ and $2\ell 2\nu$ channels.

| Parameter | Observed | Expected |
|----------------------------|-------------------------------------|-------------------------------------|
| $\mu^{\text{off-shell}}$ | $0.67^{+0.42}_{-0.32} [0.14, 1.54]$ | $1.00^{+0.83}_{-0.84} [0.02, 2.46]$ |
| $\mu_F^{\text{off-shell}}$ | $0.57^{+0.50}_{-0.36} [0.04, 1.61]$ | $1.00^{+0.90}_{-0.98} [<2.62]$ |
| $\mu_V^{\text{off-shell}}$ | $0.87^{+0.93}_{-0.57} [0.05, 2.90]$ | $1.00^{+1.95}_{-0.89} [<4.34]$ |

12 Summary

A measurement of the Higgs boson mass (m_H) and width (Γ_H) using the decays to two Z bosons is presented. The data sample comes from proton-proton collisions at the LHC recorded by the CMS experiment at a center-of-mass energy of 13 TeV, corresponding to an integrated

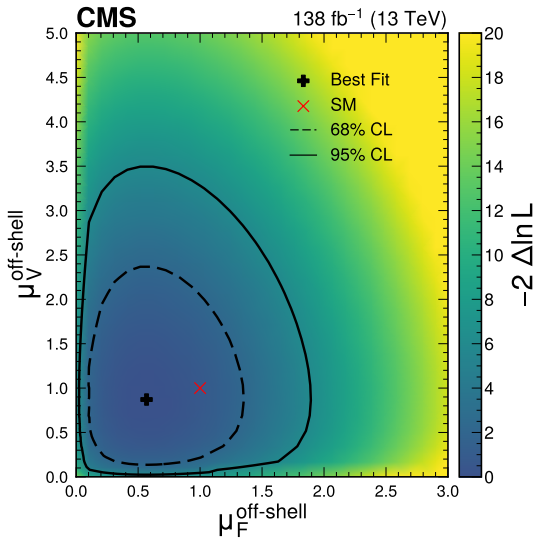


Figure 12: Observed 2D profile likelihood projection of the off-shell signal strength parameters ($\mu_F^{\text{off-shell}}$, $\mu_V^{\text{off-shell}}$) from the fit to the combined off-shell $H \rightarrow ZZ \rightarrow 4\ell$ and $2\ell 2\nu$ channels. The best fit value is shown by the black cross and the SM prediction by the red x. The 68 and 95% CL contours are given by the dashed and solid curves, respectively. The color scale to the right of the plot relates the quantitative values.

luminosity of 138 fb^{-1} . On-shell Higgs boson production with the $H \rightarrow 4\ell$ decay ($\ell = e, \mu$) is used to measure its mass and constrain its width. The mass measurement yields $m_H = 125.04 \pm 0.11 \text{ (stat)} \pm 0.05 \text{ (syst)} \text{ GeV} = 125.04 \pm 0.12 \text{ GeV}$, in agreement with the expected precision of $\pm 0.12 \text{ GeV}$. From on-shell production events, an upper limit of $\Gamma_H < 330 \text{ MeV}$ is set at 95% confidence level. The mass measurement is further improved combining data from Runs 1 and 2, leading to the most precise single measurement of the mass to date in this channel, $m_H = 125.08 \pm 0.10 \text{ (stat)} \pm 0.05 \text{ (syst)} \text{ GeV} = 125.08 \pm 0.12 \text{ GeV}$. Using on- and off-shell Higgs boson production with the decay to four leptons, and combining them with a separate analysis with Higgs boson decay to two leptons plus two neutrinos, we measure $\Gamma_H = 3.0^{+2.0}_{-1.5} \text{ MeV}$, consistent with the standard model prediction of 4.1 MeV . These results are summarized in Table 8. The strength of the off-shell Higgs boson production is also reported, and the scenario of no off-shell Higgs boson production is excluded at a confidence level corresponding to 3.8 standard deviations. Results of the measurements are tabulated in the HEPData record for this analysis [97].

Acknowledgments

We congratulate our colleagues in the CERN accelerator departments for the excellent performance of the LHC and thank the technical and administrative staffs at CERN and at other CMS institutes for their contributions to the success of the CMS effort. In addition, we gratefully acknowledge the computing centers and personnel of the Worldwide LHC Computing Grid and other centers for delivering so effectively the computing infrastructure essential to our analyses. Finally, we acknowledge the enduring support for the construction and operation of the LHC, the CMS detector, and the supporting computing infrastructure provided by the following funding agencies: SC (Armenia), BMBWF and FWF (Austria); FNRS and FWO (Belgium); CNPq, CAPES, FAPERJ, FAPERGS, and FAPESP (Brazil); MES and BNSF (Bulgaria); CERN; CAS, MoST, and NSFC (China); MINCIENCIAS (Colombia); MSES and CSF

Table 8: Summary of the Higgs boson mass and total width Γ_H measurements, showing the allowed 68% CL (central values with uncertainties) and 95% CL (in square brackets) intervals. Uncertainties are reported as a combination of statistical and systematic uncertainties. The first two rows display the outcomes of the analysis conducted within the on-shell $H \rightarrow ZZ \rightarrow 4\ell$ region, where the width is restricted to be positive. The third row incorporates results from the off-shell $H \rightarrow ZZ \rightarrow 4\ell$ region combined with the on-shell $H \rightarrow ZZ \rightarrow 4\ell$ [83] and off-shell $H \rightarrow ZZ \rightarrow 2\ell 2\nu$ [24].

| Parameter | Observed | Expected |
|----------------------------|--------------------------------|---------------------------|
| m_H (GeV) | 125.08 ± 0.12 | ± 0.12 |
| on-shell Γ_H (MeV) | <50 [<330] | <320 [<640] |
| off-shell Γ_H (MeV) | $3.0^{+2.0}_{-1.5}$ [0.6, 7.3] | 4.1 ± 3.5 [0.1, 10.5] |

(Croatia); RIF (Cyprus); SENESCYT (Ecuador); ERC PRG, RVTT3 and MoER TK202 (Estonia); Academy of Finland, MEC, and HIP (Finland); CEA and CNRS/IN2P3 (France); SRNSF (Georgia); BMBF, DFG, and HGF (Germany); GSRI (Greece); NKFIH (Hungary); DAE and DST (India); IPM (Iran); SFI (Ireland); INFN (Italy); MSIP and NRF (Republic of Korea); MES (Latvia); LMTLT (Lithuania); MOE and UM (Malaysia); BUAP, CINVESTAV, CONACYT, LNS, SEP, and UASLP-FAI (Mexico); MOS (Montenegro); MBIE (New Zealand); PAEC (Pakistan); MES and NSC (Poland); FCT (Portugal); MESTD (Serbia); MCIN/AEI and PCTI (Spain); MOSTR (Sri Lanka); Swiss Funding Agencies (Switzerland); MST (Taipei); MHESI and NSTDA (Thailand); TUBITAK and TENMAK (Turkey); NASU (Ukraine); STFC (United Kingdom); DOE and NSF (USA).

Individuals have received support from the Marie-Curie program and the European Research Council and Horizon 2020 Grant, contract Nos. 675440, 724704, 752730, 758316, 765710, 824093, 101115353, 101002207, and COST Action CA16108 (European Union); the Leventis Foundation; the Alfred P. Sloan Foundation; the Alexander von Humboldt Foundation; the Science Committee, project no. 22rl-037 (Armenia); the Belgian Federal Science Policy Office; the Fonds pour la Formation à la Recherche dans l’Industrie et dans l’Agriculture (FRIA-Belgium); the F.R.S.-FNRS and FWO (Belgium) under the “Excellence of Science – EOS” – be.h project n. 30820817; the Beijing Municipal Science & Technology Commission, No. Z191100007219010 and Fundamental Research Funds for the Central Universities (China); the Ministry of Education, Youth and Sports (MEYS) of the Czech Republic; the Shota Rustaveli National Science Foundation, grant FR-22-985 (Georgia); the Deutsche Forschungsgemeinschaft (DFG), among others, under Germany’s Excellence Strategy – EXC 2121 “Quantum Universe” – 390833306, and under project number 400140256 - GRK2497; the Hellenic Foundation for Research and Innovation (HFRI), Project Number 2288 (Greece); the Hungarian Academy of Sciences, the New National Excellence Program - ÚNKP, the NKFIH research grants K 131991, K 133046, K 138136, K 143460, K 143477, K 146913, K 146914, K 147048, 2020-2.2.1-ED-2021-00181, and TKP2021-NKTA-64 (Hungary); the Council of Science and Industrial Research, India; ICSC – National Research Center for High Performance Computing, Big Data and Quantum Computing and FAIR – Future Artificial Intelligence Research, funded by the NextGenerationEU program (Italy); the Latvian Council of Science; the Ministry of Education and Science, project no. 2022/WK/14, and the National Science Center, contracts Opus 2021/41/B/ST2/01369 and 2021/43/B/ST2/01552 (Poland); the Fundação para a Ciência e a Tecnologia, grant CEECIND/01334/2018 (Portugal); the National Priorities Research Program by Qatar National Research Fund; MCIN/AEI/10.13039/501100011033, ERDF “a way of making Europe”, and

the Programa Estatal de Fomento de la Investigación Científica y Técnica de Excelencia María de Maeztu, grant MDM-2017-0765 and Programa Severo Ochoa del Principado de Asturias (Spain); the Chulalongkorn Academic into Its 2nd Century Project Advancement Project, and the National Science, Research and Innovation Fund via the Program Management Unit for Human Resources & Institutional Development, Research and Innovation, grant B39G670016 (Thailand); the Kavli Foundation; the Nvidia Corporation; the SuperMicro Corporation; the Welch Foundation, contract C-1845; and the Weston Havens Foundation (USA).

References

- [1] S. L. Glashow, "Partial-symmetries of weak interactions", *Nucl. Phys.* **22** (1961) 579, doi:10.1016/0029-5582(61)90469-2.
- [2] F. Englert and R. Brout, "Broken symmetry and the mass of gauge vector mesons", *Phys. Rev. Lett.* **13** (1964) 321, doi:10.1103/PhysRevLett.13.321.
- [3] P. W. Higgs, "Broken symmetries, massless particles and gauge fields", *Phys. Lett.* **12** (1964) 132, doi:10.1016/0031-9163(64)91136-9.
- [4] P. W. Higgs, "Broken symmetries and the masses of gauge bosons", *Phys. Rev. Lett.* **13** (1964) 508, doi:10.1103/PhysRevLett.13.508.
- [5] G. S. Guralnik, C. R. Hagen, and T. W. B. Kibble, "Global conservation laws and massless particles", *Phys. Rev. Lett.* **13** (1964) 585, doi:10.1103/PhysRevLett.13.585.
- [6] S. Weinberg, "A model of leptons", *Phys. Rev. Lett.* **19** (1967) 1264, doi:10.1103/PhysRevLett.19.1264.
- [7] A. Salam, "Weak and electromagnetic interactions", in *Elementary particle physics: relativistic groups and analyticity*, N. Svartholm, ed., p. 367. Almqvist & Wiksell, Stockholm, 1968. Proceedings of the eighth Nobel symposium.
- [8] ATLAS Collaboration, "Observation of a new particle in the search for the Standard Model Higgs boson with the ATLAS detector at the LHC", *Phys. Lett. B* **716** (2012) 1, doi:10.1016/j.physletb.2012.08.020, arXiv:1207.7214.
- [9] CMS Collaboration, "Observation of a new boson at a mass of 125 GeV with the CMS experiment at the LHC", *Phys. Lett. B* **716** (2012) 30, doi:10.1016/j.physletb.2012.08.021, arXiv:1207.7235.
- [10] CMS Collaboration, "Observation of a new boson with mass near 125 GeV in pp collisions at $\sqrt{s} = 7$ and 8 TeV", *JHEP* **06** (2013) 081, doi:10.1007/JHEP06(2013)081, arXiv:1303.4571.
- [11] ATLAS Collaboration, "A detailed map of Higgs boson interactions by the atlas experiment ten years after the discovery", *Nature* **607** (2022) 52, doi:10.1038/s41586-022-04893-w.
- [12] CMS Collaboration, "A portrait of the Higgs boson by the CMS experiment ten years after the discovery", *Nature* **607** (2022) 60, doi:10.1038/s41586-022-04892-x.
- [13] LHC Higgs Cross Section Working Group, "Handbook of LHC Higgs cross sections: 4. deciphering the nature of the Higgs sector", *CERN* (2016) doi:10.23731/CYRM-2017-002, arXiv:1610.07922.

- [14] ATLAS and CMS Collaborations, “Combined measurement of the Higgs boson mass in pp collisions at $\sqrt{s} = 7$ and 8 TeV with the ATLAS and CMS experiments”, *Phys. Rev. Lett.* **114** (2015) 191803, doi:10.1103/PhysRevLett.114.191803, arXiv:1503.07589.
- [15] ATLAS Collaboration, “Combined measurement of the Higgs boson mass from the $H \rightarrow \gamma\gamma$ and $H \rightarrow ZZ^* \rightarrow 4\ell$ decay channels with the ATLAS detector using $\sqrt{s} = 7, 8$ and 13 TeV pp collision data”, *Phys. Rev. Lett.* **131** (2023) 251802, doi:10.1103/PhysRevLett.131.251802, arXiv:2308.04775.
- [16] CMS Collaboration, “Precise determination of the mass of the Higgs boson and tests of compatibility of its couplings with the standard model predictions using proton collisions at 7 and 8 TeV”, *Eur. Phys. J. C* **75** (2015) 212, doi:10.1140/epjc/s10052-015-3351-7, arXiv:1412.8662.
- [17] CMS Collaboration, “Measurements of properties of the Higgs boson decaying into the four-lepton final state in pp collisions at $\sqrt{s} = 13$ TeV”, *JHEP* **11** (2017) 047, doi:10.1007/JHEP11(2017)047, arXiv:1706.09936.
- [18] CMS Collaboration, “Constraints on the Higgs boson width from off-shell production and decay to Z-boson pairs”, *Phys. Lett. B* **736** (2014) 64, doi:10.1016/j.physletb.2014.06.077, arXiv:1405.3455.
- [19] ATLAS Collaboration, “Constraints on the off-shell Higgs boson signal strength in the high-mass ZZ and WW final states with the ATLAS detector”, *Eur. Phys. J. C* **75** (2015) 335, doi:10.1140/epjc/s10052-015-3542-2, arXiv:1503.01060.
- [20] CMS Collaboration, “Limits on the Higgs boson lifetime and width from its decay to four charged leptons”, *Phys. Rev. D* **92** (2015) 072010, doi:10.1103/PhysRevD.92.072010, arXiv:1507.06656.
- [21] CMS Collaboration, “Search for Higgs boson off-shell production in proton-proton collisions at 7 and 8 TeV and derivation of constraints on its total decay width”, *JHEP* **09** (2016) 051, doi:10.1007/JHEP09(2016)051, arXiv:1605.02329.
- [22] ATLAS Collaboration, “Constraints on off-shell Higgs boson production and the Higgs boson total width in $ZZ \rightarrow 4\ell$ and $ZZ \rightarrow 2\ell 2\nu$ final states with the ATLAS detector”, *Phys. Lett. B* **786** (2018) 223, doi:10.1016/j.physletb.2018.09.048, arXiv:1808.01191.
- [23] CMS Collaboration, “Measurements of the Higgs boson width and anomalous HVV couplings from on-shell and off-shell production in the four-lepton final state”, *Phys. Rev. D* (2019) 112003, doi:10.1103/PhysRevD.99.112003, arXiv:1901.00174.
- [24] CMS Collaboration, “Measurement of the Higgs boson width and evidence of its off-shell contributions to ZZ production”, *Nature Phys.* **18** (2022) 1329, doi:10.1038/s41567-022-01682-0, arXiv:2202.06923.
- [25] F. Caola and K. Melnikov, “Constraining the Higgs boson width with ZZ production at the LHC”, *Phys. Rev. D* **88** (2013) 054024, doi:10.1103/PhysRevD.88.054024, arXiv:1307.4935.
- [26] N. Kauer and G. Passarino, “Inadequacy of zero-width approximation for a light Higgs boson signal”, *JHEP* **08** (2012) 116, doi:10.1007/JHEP08(2012)116, arXiv:1206.4803.

- [27] J. M. Campbell, R. K. Ellis, and C. Williams, “Bounding the Higgs width at the LHC using full analytic results for $gg \rightarrow e^-e^+\mu^-\mu^+$ ”, *JHEP* **04** (2014) 060, doi:10.1007/JHEP04(2014)060, arXiv:1311.3589.
- [28] ATLAS Collaboration, “Evidence of off-shell Higgs boson production from ZZ leptonic decay channels and constraints on its total width with the ATLAS detector”, *Phys. Lett. B* **846** (2023) 138223, doi:10.1016/j.physletb.2023.138223, arXiv:2304.01532.
- [29] B. W. Lee, C. Quigg, and H. B. Thacker, “Strength of weak interactions at very high-energies and the Higgs boson mass”, *Phys. Rev. Lett.* **38** (1977) 883, doi:10.1103/PhysRevLett.38.883.
- [30] CMS Collaboration, “Search for a new scalar resonance decaying to a pair of Z bosons in proton-proton collisions at $\sqrt{s} = 13$ TeV”, *JHEP* **06** (2018) 127, doi:10.1007/JHEP06(2018)127, arXiv:1804.01939.
- [31] CMS Collaboration, “The CMS experiment at the CERN LHC”, *JINST* **3** (2008) S08004, doi:10.1088/1748-0221/3/08/S08004.
- [32] CMS Collaboration, “Development of the CMS detector for the CERN LHC Run 3”, *JINST* **19** (2024) P05064, doi:10.1088/1748-0221/19/05/P05064.
- [33] CMS Collaboration, “Performance of the CMS Level-1 trigger in proton-proton collisions at $\sqrt{s} = 13$ TeV”, *JINST* **15** (2020) P10017, doi:10.1088/1748-0221/15/10/P10017, arXiv:2006.10165.
- [34] CMS Collaboration, “The CMS trigger system”, *JINST* **12** (2017) P01020, doi:10.1088/1748-0221/12/01/P01020, arXiv:1609.02366.
- [35] CMS Collaboration, “Technical proposal for the phase-II upgrade of the CMS detector”, CMS Technical proposal CERN-LHCC-2015-010, CMS-TDR-15-02, CERN, 2015.
- [36] CMS Collaboration, “Electron and photon reconstruction and identification with the CMS experiment at the CERN LHC”, *JINST* **16** (2021) P05014, doi:10.1088/1748-0221/16/05/p05014, arXiv:2012.06888.
- [37] CMS Collaboration, “ECAL 2016 refined calibration and Run 2 summary plots”, CMS Detector Performance Summary CMS-DP-2020-021, CERN, 2020.
- [38] CMS Collaboration, “Performance of the CMS muon detector and muon reconstruction with proton-proton collisions at $\sqrt{s} = 13$ TeV”, *JINST* **13** (2018) P06015, doi:10.1088/1748-0221/13/06/p06015, arXiv:1804.04528.
- [39] CMS Collaboration, “Measurements of production cross sections of the Higgs boson in the four-lepton final state in proton–proton collisions at $\sqrt{s} = 13$ TeV”, *Eur. Phys. J. C* **81** (2021) 488, doi:10.1140/epjc/s10052-021-09200-x, arXiv:2103.04956.
- [40] S. Frixione, P. Nason, and C. Oleari, “Matching NLO QCD computations with parton shower simulations: the POWHEG method”, *JHEP* **11** (2007) 070, doi:10.1088/1126-6708/2007/11/070, arXiv:0709.2092.
- [41] E. Bagnaschi, G. Degrassi, P. Slavich, and A. Vicini, “Higgs production via gluon fusion in the POWHEG approach in the SM and in the MSSM”, *JHEP* **02** (2012) 088, doi:10.1007/JHEP02(2012)088, arXiv:1111.2854.

- [42] P. Nason and C. Oleari, “NLO Higgs boson production via vector-boson fusion matched with shower in POWHEG”, *JHEP* **02** (2010) 037, doi:10.1007/JHEP02(2010)037, arXiv:0911.5299.
- [43] G. Luisoni, P. Nason, C. Oleari, and F. Tramontano, “ $\text{HW}^\pm/\text{HZ} + 0$ and 1 jet at NLO with the POWHEG BOX interfaced to GoSam and their merging within MiNLO”, *JHEP* **10** (2013) 083, doi:10.1007/JHEP10(2013)083, arXiv:1306.2542.
- [44] H. B. Hartanto, B. Jager, L. Reina, and D. Wackerlo, “Higgs boson production in association with top quarks in the POWHEG BOX”, *Phys. Rev. D* **91** (2015) 094003, doi:10.1103/PhysRevD.91.094003, arXiv:1501.04498.
- [45] P. Nason, “A new method for combining NLO QCD with shower Monte Carlo algorithms”, *JHEP* **11** (2004) 040, doi:10.1088/1126-6708/2004/11/040, arXiv:hep-ph/0409146.
- [46] S. Alioli, P. Nason, C. Oleari, and E. Re, “A general framework for implementing NLO calculations in shower Monte Carlo programs: the POWHEG BOX”, *JHEP* **06** (2010) 043, doi:10.1007/JHEP06(2010)043, arXiv:1002.2581.
- [47] K. Hamilton, P. Nason, and G. Zanderighi, “MINLO: multi-scale improved NLO”, *JHEP* **10** (2012) 155, doi:10.1007/JHEP10(2012)155, arXiv:1206.3572.
- [48] Y. Gao et al., “Spin determination of single-produced resonances at hadron colliders”, *Phys. Rev. D* **81** (2010) 075022, doi:10.1103/PhysRevD.81.075022, arXiv:1001.3396.
- [49] S. Bolognesi et al., “Spin and parity of a single-produced resonance at the LHC”, *Phys. Rev. D* **86** (2012) 095031, doi:10.1103/PhysRevD.86.095031, arXiv:1208.4018.
- [50] I. Anderson et al., “Constraining anomalous HVV interactions at proton and lepton colliders”, *Phys. Rev. D* **89** (2014) 035007, doi:10.1103/PhysRevD.89.035007, arXiv:1309.4819.
- [51] A. V. Gritsan, R. Röntsch, M. Schulze, and M. Xiao, “Constraining anomalous Higgs boson couplings to the heavy flavor fermions using matrix element techniques”, *Phys. Rev. D* **94** (2016) 055023, doi:10.1103/PhysRevD.94.055023, arXiv:1606.03107.
- [52] A. V. Gritsan et al., “New features in the JHU generator framework: constraining Higgs boson properties from on-shell and off-shell production”, *Phys. Rev. D* **102** (2020) 056022, doi:10.1103/PhysRevD.102.056022, arXiv:2002.09888.
- [53] J. M. Campbell and R. K. Ellis, “MCFM for the Tevatron and the LHC”, *Nucl. Phys. Proc. Suppl.* **205-206** (2010) 10, doi:10.1016/j.nuclphysbps.2010.08.011, arXiv:1007.3492.
- [54] J. M. Campbell, R. K. Ellis, and C. Williams, “Vector boson pair production at the LHC”, *JHEP* **07** (2011) 018, doi:10.1007/JHEP07(2011)018, arXiv:1105.0020.
- [55] J. M. Campbell and R. K. Ellis, “Higgs constraints from vector boson fusion and scattering”, *JHEP* **04** (2015) 030, doi:10.1007/JHEP04(2015)030, arXiv:1502.02990.

- [56] A. Ballestrero et al., “PHANTOM: a Monte Carlo event generator for six parton final states at high energy colliders”, *Comput. Phys. Commun.* **180** (2009) 401, doi:10.1016/j.cpc.2008.10.005, arXiv:0801.3359.
- [57] S. Catani and M. Grazzini, “An NNLO subtraction formalism in hadron collisions and its application to Higgs boson production at the LHC”, *Phys. Rev. Lett.* **98** (2007) 222002, doi:10.1103/PhysRevLett.98.222002, arXiv:hep-ph/0703012.
- [58] M. Grazzini, “NNLO predictions for the Higgs boson signal in the $H \rightarrow WW \rightarrow \ell\nu\ell\nu$ and $H \rightarrow ZZ \rightarrow 4\ell$ decay channels”, *JHEP* **02** (2008) 043, doi:10.1088/1126-6708/2008/02/043, arXiv:0801.3232.
- [59] M. Grazzini and H. Sargsyan, “Heavy-quark mass effects in Higgs boson production at the LHC”, *JHEP* **09** (2013) 129, doi:10.1007/JHEP09(2013)129, arXiv:1306.4581.
- [60] F. Caola, K. Melnikov, R. Röntsch, and L. Tancredi, “QCD corrections to ZZ production in gluon fusion at the LHC”, *Phys. Rev. D* **92** (2015) 094028, doi:10.1103/PhysRevD.92.094028, arXiv:1509.06734.
- [61] K. Melnikov and M. Dowling, “Production of two Z-bosons in gluon fusion in the heavy top quark approximation”, *Phys. Lett. B* **744** (2015) 43, doi:10.1016/j.physletb.2015.03.030, arXiv:1503.01274.
- [62] J. M. Campbell, R. K. Ellis, M. Czakon, and S. Kirchner, “Two loop correction to interference in $gg \rightarrow ZZ$ ”, *JHEP* **08** (2016) 011, doi:10.1007/JHEP08(2016)011, arXiv:1605.01380.
- [63] F. Caola et al., “QCD corrections to vector boson pair production in gluon fusion including interference effects with off-shell Higgs at the LHC”, *JHEP* **07** (2016) 087, doi:10.1007/JHEP07(2016)087, arXiv:1605.04610.
- [64] M. Grazzini, S. Kallweit, and D. Rathlev, “ZZ production at the LHC: fiducial cross sections and distributions in NNLO QCD”, *Phys. Lett. B* **750** (2015) 407, doi:10.1016/j.physletb.2015.09.055, arXiv:1507.06257.
- [65] A. Bierweiler, T. Kasprzik, and J. H. Kühn, “Vector-boson pair production at the LHC to $\mathcal{O}(\alpha^3)$ accuracy”, *JHEP* **12** (2013) 071, doi:10.1007/JHEP12(2013)071, arXiv:1305.5402.
- [66] J. Alwall et al., “The automated computation of tree-level and next-to-leading order differential cross sections, and their matching to parton shower simulations”, *JHEP* **07** (2014) 079, doi:10.1007/JHEP07(2014)079, arXiv:1405.0301.
- [67] T. Sjöstrand et al., “An introduction to PYTHIA 8.2”, *Comput. Phys. Commun.* **191** (2015) 159, doi:10.1016/j.cpc.2015.01.024, arXiv:1410.3012.
- [68] CMS Collaboration, “Event generator tunes obtained from underlying event and multiparton scattering measurements”, *Eur. Phys. J. C* **76** (2016) 155, doi:10.1140/epjc/s10052-016-3988-x, arXiv:1512.00815.
- [69] CMS Collaboration, “Extraction and validation of a new set of CMS PYTHIA8 tunes from underlying-event measurements”, *Eur. Phys. J. C* **80** (2020) 4, doi:10.1140/epjc/s10052-019-7499-4, arXiv:1903.12179.

- [70] NNPDF Collaboration, “Unbiased global determination of parton distributions and their uncertainties at NNLO and at LO”, *Nucl. Phys. B* **855** (2012) 153,
`doi:10.1016/j.nuclphysb.2011.09.024`, `arXiv:1107.2652`.
- [71] GEANT4 Collaboration, “GEANT4 — a simulation toolkit”, *Nucl. Instrum. Meth. A* **506** (2003) 250, `doi:10.1016/S0168-9002(03)01368-8`.
- [72] CMS Collaboration, “Particle-flow reconstruction and global event description with the CMS detector”, *JINST* **12** (2017) P10003, `doi:10.1088/1748-0221/12/10/P10003`,
`arXiv:1706.04965`.
- [73] CMS Collaboration, “Pileup mitigation at CMS in 13 TeV data”, *JINST* **15** (2020) P09018,
`doi:10.1088/1748-0221/15/09/P09018`, `arXiv:2003.00503`.
- [74] T. Chen and C. Guestrin, “XGBoost: A scalable tree boosting system”, 2016.
`arXiv:1603.02754`.
- [75] CMS Collaboration, “Measurements of inclusive and differential cross sections for the Higgs boson production and decay to four-leptons in proton-proton collisions at $\sqrt{s} = 13$ TeV”, *JHEP* **08** (2023) 040, `doi:10.1007/JHEP08(2023)040`, `arXiv:2305.07532`.
- [76] CMS Collaboration, “Measurement of the inclusive W and Z production cross sections in pp collisions at $\sqrt{s} = 7$ TeV”, *JHEP* **10** (2011) 132, `doi:10.1007/JHEP10(2011)132`,
`arXiv:1107.4789`.
- [77] A. Bodek et al., “Extracting muon momentum scale corrections for hadron collider experiments”, *Eur. Phys. J. C* **72** (2012) `doi:10.1140/epjc/s10052-012-2194-8`.
- [78] M. Cacciari, G. P. Salam, and G. Soyez, “The anti- k_T jet clustering algorithm”, *JHEP* **04** (2008) 063, `doi:10.1088/1126-6708/2008/04/063`, `arXiv:0802.1189`.
- [79] M. Cacciari, G. P. Salam, and G. Soyez, “FastJet user manual”, *Eur. Phys. J. C* **72** (2012) 1896, `doi:10.1140/epjc/s10052-012-1896-2`, `arXiv:1111.6097`.
- [80] CMS Collaboration, “Identification of heavy-flavour jets with the CMS detector in pp collisions at 13 TeV”, *JINST* **13** (2018) P05011,
`doi:10.1088/1748-0221/13/05/P05011`, `arXiv:1712.07158`.
- [81] T. Skwarnicki, “A study of the radiative CASCADE transitions between the Upsilon-Prime and Upsilon resonances”. PhD thesis, Cracow, INP, 1986.
- [82] CMS Collaboration, “Constraints on anomalous Higgs boson couplings using production and decay information in the four-lepton final state”, *Phys. Lett. B* **775** (2017) 1,
`doi:10.1016/j.physletb.2017.10.021`, `arXiv:1707.00541`.
- [83] CMS Collaboration, “Constraints on anomalous Higgs boson couplings to vector bosons and fermions in its production and decay using the four-lepton final state”, *Phys. Rev. D* **104** (2021) 052004, `doi:10.1103/PhysRevD.104.052004`, `arXiv:2104.12152`.
- [84] M. Oreglia, “A study of the reactions $\psi' \rightarrow \gamma\gamma\psi$ ”. PhD thesis, Stanford University, 1980.
SLAC Report SLAC-R-236.
- [85] CMS Collaboration, “Precision luminosity measurement in proton-proton collisions at $\sqrt{s} = 13$ TeV in 2015 and 2016 at CMS”, *Eur. Phys. J. C* **81** (2021) 800,
`doi:10.1140/epjc/s10052-021-09538-2`, `arXiv:2104.01927`.

- [86] CMS Collaboration, “CMS luminosity measurement for the 2017 data-taking period at $\sqrt{s} = 13$ TeV”, CMS Physics Analysis Summary CMS-PAS-LUM-17-004, CERN, 2018.
- [87] CMS Collaboration, “CMS luminosity measurement for the 2018 data-taking period at $\sqrt{s} = 13$ TeV”, CMS Physics Analysis Summary CMS-PAS-LUM-18-002, CERN, 2019.
- [88] CMS Collaboration, “A measurement of the Higgs boson mass in the diphoton decay channel”, *Phys. Lett. B* **805** (2020) 135425, doi:10.1016/j.physletb.2020.135425, arXiv:2002.06398.
- [89] Particle Data Group, K. A. Olive et al., “Review of Particle Physics”, *Chin. Phys. C* **38** (2014) 090001, doi:10.1088/1674-1137/38/9/090001.
- [90] CMS Collaboration, “Measurement of the properties of a Higgs boson in the four-lepton final state”, *Phys. Rev. D* **89** (2014) 092007, doi:10.1103/PhysRevD.89.092007, arXiv:1312.5353.
- [91] G. J. Feldman and R. D. Cousins, “Unified approach to the classical statistical analysis of small signals”, *Phys. Rev. D* **57** (1998) 3873, doi:10.1103/PhysRevD.57.3873, arXiv:physics/9711021.
- [92] CMS Collaboration, “The CMS statistical analysis and combination tool: COMBINE”, 2024. arXiv:2404.06614. Submitted to *Comput. Softw. Big Sci.*
- [93] W. Verkerke and D. P. Kirkby, “The RooFit toolkit for data modeling”, in *Proceedings of the 13th International Conference for Computing in High-Energy and Nuclear Physics (CHEP03)*. 2003. arXiv:physics/0306116.
- [94] R. Brun and F. Rademakers, “ROOT: An object oriented data analysis framework”, *Nucl. Instrum. Meth. A* **389** (1997) 81, doi:10.1016/S0168-9002(97)00048-X.
- [95] S. S. Wilks, “The large-sample distribution of the likelihood ratio for testing composite hypotheses”, *Annals Math. Statist.* **9** (1938) 60, doi:10.1214/aoms/1177732360.
- [96] J. Davis et al., “Constraining anomalous Higgs boson couplings to virtual photons”, *Phys. Rev. D* **105** (2022) 096027, doi:10.1103/PhysRevD.105.096027, arXiv:2109.13363.
- [97] “HEPData record for this analysis”, 2024. doi:10.17182/hepdata.153670.

A The CMS Collaboration

Yerevan Physics Institute, Yerevan, Armenia

A. Hayrapetyan, A. Tumasyan¹ 

Institut für Hochenergiephysik, Vienna, Austria

W. Adam , J.W. Andrejkovic, T. Bergauer , S. Chatterjee , K. Damanakis , M. Dragicevic , P.S. Hussain , M. Jeitler² , N. Krammer , A. Li , D. Liko , I. Mikulec , J. Schieck² , R. Schöfbeck , D. Schwarz , M. Sonawane , S. Templ , W. Waltenberger , C.-E. Wulz²

Universiteit Antwerpen, Antwerpen, Belgium

M.R. Darwish³ , T. Janssen , T. Van Laer, P. Van Mechelen 

Vrije Universiteit Brussel, Brussel, Belgium

N. Breugelmans, J. D'Hondt , S. Dansana , A. De Moor , M. Delcourt , F. Heyen, S. Lowette , I. Makarenko , D. Müller , S. Tavernier , M. Tytgat⁴ , G.P. Van Onsem , S. Van Putte , D. Vannerom

Université Libre de Bruxelles, Bruxelles, Belgium

B. Bilin , B. Clerbaux , A.K. Das, G. De Lentdecker , H. Evard , L. Favart , P. Gianneios , J. Jaramillo , A. Khalilzadeh, F.A. Khan , K. Lee , M. Mahdavikhorrami , A. Malara , S. Paredes , M.A. Shahzad, L. Thomas , M. Vanden Bemden , C. Vander Velde , P. Vanlaer

Ghent University, Ghent, Belgium

M. De Coen , D. Dobur , G. Gokbulut , Y. Hong , J. Knolle , L. Lambrecht , D. Marckx , K. Mota Amarilo , A. Samalan, K. Skovpen , N. Van Den Bossche , J. van der Linden , L. Wezenbeek

Université Catholique de Louvain, Louvain-la-Neuve, Belgium

A. Benecke , A. Bethani , G. Bruno , C. Caputo , J. De Favereau De Jeneret , C. Delaere , I.S. Donertas , A. Giammanco , A.O. Guzel , Sa. Jain , V. Lemaitre, J. Lidrych , P. Mastrapasqua , T.T. Tran , S. Wertz

Centro Brasileiro de Pesquisas Fisicas, Rio de Janeiro, Brazil

G.A. Alves , M. Alves Gallo Pereira , E. Coelho , G. Correia Silva , C. Hensel , T. Menezes De Oliveira , C. Mora Herrera⁵ , A. Moraes , P. Rebello Teles , M. Soeiro, A. Vilela Pereira⁵

Universidade do Estado do Rio de Janeiro, Rio de Janeiro, Brazil

W.L. Aldá Júnior , M. Barroso Ferreira Filho , H. Brandao Malbouisson , W. Carvalho , J. Chinellato⁶, E.M. Da Costa , G.G. Da Silveira⁷ , D. De Jesus Damiao , S. Fonseca De Souza , R. Gomes De Souza, M. Macedo , J. Martins⁸ , L. Mundim , H. Nogima , J.P. Pinheiro , A. Santoro , A. Sznajder , M. Thiel

Universidade Estadual Paulista, Universidade Federal do ABC, São Paulo, Brazil

C.A. Bernardes⁷ , L. Calligaris , T.R. Fernandez Perez Tomei , E.M. Gregores , B. Lopes Da Costa, I. Maietto Silverio , P.G. Mercadante , S.F. Novaes , B. Orzari , Sandra S. Padula 

Institute for Nuclear Research and Nuclear Energy, Bulgarian Academy of Sciences, Sofia, Bulgaria

A. Aleksandrov , G. Antchev , R. Hadjiiska , P. Iaydjiev , M. Misheva , M. Shopova , G. Sultanov 

University of Sofia, Sofia, Bulgaria

A. Dimitrov , L. Litov , B. Pavlov , P. Petkov , A. Petrov , E. Shumka 

Instituto De Alta Investigación, Universidad de Tarapacá, Casilla 7 D, Arica, Chile

S. Keshri , S. Thakur 

Beihang University, Beijing, China

T. Cheng , T. Javaid , L. Yuan 

Department of Physics, Tsinghua University, Beijing, China

Z. Hu , Z. Liang, J. Liu, K. Yi^{9,10} 

Institute of High Energy Physics, Beijing, China

G.M. Chen¹¹ , H.S. Chen¹¹ , M. Chen¹¹ , F. Iemmi , A. Kapoor¹² , H. Liao , Z.-A. Liu¹³ , R. Sharma¹⁴ , J.N. Song¹³, J. Tao , C. Wang¹¹, J. Wang , Z. Wang¹¹, C. Zhang¹¹, H. Zhang , J. Zhao 

State Key Laboratory of Nuclear Physics and Technology, Peking University, Beijing, China

A. Agapitos , Y. Ban , S. Deng , B. Guo, C. Jiang , A. Levin , C. Li , Q. Li , Y. Mao, S. Qian, S.J. Qian , X. Qin, X. Sun , D. Wang , H. Yang, L. Zhang , Y. Zhao, C. Zhou 

Guangdong Provincial Key Laboratory of Nuclear Science and Guangdong-Hong Kong Joint Laboratory of Quantum Matter, South China Normal University, Guangzhou, China

S. Yang 

Sun Yat-Sen University, Guangzhou, China

Z. You 

University of Science and Technology of China, Hefei, China

K. Jaffel , N. Lu 

Nanjing Normal University, Nanjing, China

G. Bauer¹⁵, B. Li, J. Zhang 

Institute of Modern Physics and Key Laboratory of Nuclear Physics and Ion-beam Application (MOE) - Fudan University, Shanghai, China

X. Gao¹⁶ 

Zhejiang University, Hangzhou, Zhejiang, China

Z. Lin , C. Lu , M. Xiao 

Universidad de Los Andes, Bogota, Colombia

C. Avila , D.A. Barbosa Trujillo, A. Cabrera , C. Florez , J. Fraga , J.A. Reyes Vega

Universidad de Antioquia, Medellin, Colombia

F. Ramirez , C. Rendón, M. Rodriguez , A.A. Ruales Barbosa , J.D. Ruiz Alvarez 

University of Split, Faculty of Electrical Engineering, Mechanical Engineering and Naval Architecture, Split, Croatia

D. Giljanovic , N. Godinovic , D. Lelas , A. Sculac 

University of Split, Faculty of Science, Split, Croatia

M. Kovac , A. Petkovic, T. Sculac 

Institute Rudjer Boskovic, Zagreb, Croatia

P. Bargassa , V. Brigljevic , B.K. Chitroda , D. Ferencek , K. Jakovcic, S. Mishra , A. Starodumov¹⁷ , T. Susa 

University of Cyprus, Nicosia, Cyprus

A. Attikis , K. Christoforou , A. Hadjiagapiou, C. Leonidou , J. Mousa , C. Nicolaou, L. Paizanos, F. Ptochos , P.A. Razis , H. Rykaczewski, H. Saka , A. Stepennov 

Charles University, Prague, Czech Republic

M. Finger , M. Finger Jr. , A. Kveton 

Universidad San Francisco de Quito, Quito, Ecuador

E. Carrera Jarrin 

Academy of Scientific Research and Technology of the Arab Republic of Egypt, Egyptian Network of High Energy Physics, Cairo, Egypt

Y. Assran^{18,19}, B. El-mahdy, S. Elgammal¹⁹

Center for High Energy Physics (CHEP-FU), Fayoum University, El-Fayoum, Egypt

A. Lotfy , M.A. Mahmoud 

National Institute of Chemical Physics and Biophysics, Tallinn, Estonia

K. Ehataht , M. Kadastik, T. Lange , S. Nandan , C. Nielsen , J. Pata , M. Raidal , L. Tani , C. Veelken 

Department of Physics, University of Helsinki, Helsinki, Finland

H. Kirschenmann , K. Osterberg , M. Voutilainen 

Helsinki Institute of Physics, Helsinki, Finland

S. Bharthuar , N. Bin Norjoharuddeen , E. Brücken , F. Garcia , P. Inkaew , K.T.S. Kallonen , T. Lampén , K. Lassila-Perini , S. Lehti , T. Lindén , L. Martikainen , M. Myllymäki , M.m. Rantanen , H. Siikonen , J. Tuominiemi 

Lappeenranta-Lahti University of Technology, Lappeenranta, Finland

P. Luukka , H. Petrow 

IRFU, CEA, Université Paris-Saclay, Gif-sur-Yvette, France

M. Besancon , F. Couderc , M. Dejardin , D. Denegri, J.L. Faure, F. Ferri , S. Ganjour , P. Gras , G. Hamel de Monchenault , M. Kumar , V. Lohezic , J. Malcles , F. Orlandi , L. Portales , A. Rosowsky , M.Ö. Sahin , A. Savoy-Navarro²⁰ , P. Simkina , M. Titov , M. Tornago 

Laboratoire Leprince-Ringuet, CNRS/IN2P3, Ecole Polytechnique, Institut Polytechnique de Paris, Palaiseau, France

F. Beaudette , G. Boldrini , P. Busson , A. Cappati , C. Charlot , M. Chiusi , F. Damas , O. Davignon , A. De Wit , I.T. Ehle , B.A. Fontana Santos Alves , S. Ghosh , A. Gilbert , R. Granier de Cassagnac , A. Hakimi , B. Harikrishnan , L. Kalipoliti , G. Liu , M. Nguyen , C. Ochando , R. Salerno , J.B. Sauvan , Y. Sirois , L. Urda Gómez , E. Vernazza , A. Zabi , A. Zghiche 

Université de Strasbourg, CNRS, IPHC UMR 7178, Strasbourg, France

J.-L. Agram²¹ , J. Andrea , D. Apparu , D. Bloch , J.-M. Brom , E.C. Chabert , C. Collard , S. Falke , U. Goerlach , R. Haeberle , A.-C. Le Bihan , M. Meena , O. Ponct , G. Saha , M.A. Sessini , P. Van Hove , P. Vaucelle 

Centre de Calcul de l'Institut National de Physique Nucléaire et de Physique des Particules, CNRS/IN2P3, Villeurbanne, France

A. Di Florio 

Institut de Physique des 2 Infinis de Lyon (IP2I), Villeurbanne, France

D. Amram, S. Beauceron , B. Blancon , G. Boudoul , N. Chanon , D. Contardo , P. Depasse , C. Dozen²² , H. El Mamouni, J. Fay , S. Gascon , M. Gouzevitch , C. Greenberg, G. Grenier , B. Ille , E. Jourd'huy, I.B. Laktineh, M. Lethuillier , L. Mirabito, S. Perries, A. Purohit , M. Vander Donckt , P. Verdier , J. Xiao

Georgian Technical University, Tbilisi, Georgia

A. Khvedelidze¹⁷ , I. Lomidze , Z. Tsamalaidze¹⁷ 

RWTH Aachen University, I. Physikalisches Institut, Aachen, Germany

V. Botta , S. Consuegra Rodríguez , L. Feld , K. Klein , M. Lipinski , D. Meuser , A. Pauls , D. Pérez Adán , N. Röwert , M. Teroerde 

RWTH Aachen University, III. Physikalisches Institut A, Aachen, Germany

S. Diekmann , A. Dodonova , N. Eich , D. Eliseev , F. Engelke , J. Erdmann , M. Erdmann , P. Fackeldey , B. Fischer , T. Hebbeker , K. Hoepfner , F. Ivone , A. Jung , M.y. Lee , F. Mausolf , M. Merschmeyer , A. Meyer , S. Mukherjee , D. Noll , F. Nowotny, A. Pozdnyakov , Y. Rath, W. Redjeb , F. Rehm, H. Reithler , V. Sarkisovi , A. Schmidt , A. Sharma , J.L. Spah , A. Stein , F. Torres Da Silva De Araujo²³ , S. Wiedenbeck , S. Zaleski

RWTH Aachen University, III. Physikalisches Institut B, Aachen, Germany

C. Dziwok , G. Flügge , T. Kress , A. Nowack , O. Pooth , A. Stahl , T. Ziemons , A. Zottz 

Deutsches Elektronen-Synchrotron, Hamburg, Germany

H. Aarup Petersen , M. Aldaya Martin , J. Alimena , S. Amoroso, Y. An , J. Bach , S. Baxter , M. Bayatmakou , H. Becerril Gonzalez , O. Behnke , A. Belvedere , S. Bhattacharya , F. Blekman²⁴ , K. Borras²⁵ , A. Campbell , A. Cardini , C. Cheng, F. Colombina , M. De Silva , G. Eckerlin, D. Eckstein , L.I. Estevez Banos , O. Filatov , E. Gallo²⁴ , A. Geiser , V. Guglielmi , M. Guthoff , A. Hinzmann , L. Jeppe , B. Kaech , M. Kasemann , C. Kleinwort , R. Kogler , M. Komm , D. Krücker , W. Lange, D. Leyva Pernia , K. Lipka²⁶ , W. Lohmann²⁷ , F. Lorkowski , R. Mankel , I.-A. Melzer-Pellmann , M. Mendizabal Morentin , A.B. Meyer , G. Milella , K. Moral Figueroa , A. Mussgiller , L.P. Nair , J. Niedziela , A. Nürnberg , Y. Otarid , J. Park , E. Ranken , A. Raspereza , D. Rastorguev , J. Rübenach, L. Rygaard, A. Saggio , M. Scham^{28,25} , S. Schnake²⁵ , P. Schütze , C. Schwanenberger²⁴ , D. Selivanova , K. Sharko , M. Shchedrolosiev , D. Stafford, F. Vazzoler , A. Ventura Barroso , R. Walsh , D. Wang , Q. Wang , Y. Wen , K. Wichmann, L. Wiens²⁵ , C. Wissing , Y. Yang , A. Zimermann Castro Santos

University of Hamburg, Hamburg, Germany

A. Albrecht , S. Albrecht , M. Antonello , S. Bein , L. Benato , S. Bollweg, M. Bonanomi , P. Connor , K. El Morabit , Y. Fischer , E. Garutti , A. Grohsjean , J. Haller , H.R. Jabusch , G. Kasieczka , P. Keicher, R. Klanner , W. Korcari , T. Kramer , C.c. Kuo, V. Kutzner , F. Labe , J. Lange , A. Lobanov , C. Matthies , L. Moureaux , M. Mrowietz, A. Nigamova , Y. Nissan, A. Paasch , K.J. Pena Rodriguez , T. Quadfasel , B. Raciti , M. Rieger , D. Savoiu , J. Schindler , P. Schleper , M. Schröder , J. Schwandt , M. Sommerhalder , H. Stadie , G. Steinbrück , A. Tews, M. Wolf

Karlsruhe Institut fuer Technologie, Karlsruhe, Germany

S. Brommer , M. Burkart, E. Butz , T. Chwalek , A. Dierlamm , A. Droll, N. Faltermann , M. Giffels , A. Gottmann , F. Hartmann²⁹ , R. Hofsaess , M. Horzela 

U. Husemann , J. Kieseler , M. Klute , R. Koppenhöfer , J.M. Lawhorn , M. Link, A. Lintuluoto , B. Maier , S. Maier , S. Mitra , M. Mormile , Th. Müller , M. Neukum, M. Oh , E. Pfeffer , M. Presilla , G. Quast , K. Rabbertz , B. Regnery , N. Shadskiy , I. Shvetsov , H.J. Simonis , L. Sowa, L. Stockmeier, K. Tauqeer, M. Toms , N. Trevisani , R.F. Von Cube , M. Wassmer , S. Wieland , F. Wittig, R. Wolf , X. Zuo

Institute of Nuclear and Particle Physics (INPP), NCSR Demokritos, Aghia Paraskevi, Greece

G. Anagnostou, G. Daskalakis , A. Kyriakis, A. Papadopoulos²⁹, A. Stakia 

National and Kapodistrian University of Athens, Athens, Greece

P. Kontaxakis , G. Melachroinos, Z. Painesis , I. Papavergou , I. Paraskevas , N. Saoulidou , K. Theofilatos , E. Tziaferi , K. Vellidis , I. Zisopoulos

National Technical University of Athens, Athens, Greece

G. Bakas , T. Chatzistavrou, G. Karapostoli , K. Kousouris , I. Papakrivopoulos , E. Siamarkou, G. Tsipolitis , A. Zacharopoulou

University of Ioánnina, Ioánnina, Greece

K. Adamidis, I. Bestintzanos, I. Evangelou , C. Foudas, C. Kamtsikis, P. Katsoulis, P. Kokkas , P.G. Kosmoglou Kioseoglou , N. Manthos , I. Papadopoulos , J. Strologas 

HUN-REN Wigner Research Centre for Physics, Budapest, Hungary

C. Hajdu , D. Horvath^{30,31} , K. Márton, A.J. Rádl³² , F. Sikler , V. Veszpremi 

MTA-ELTE Lendület CMS Particle and Nuclear Physics Group, Eötvös Loránd University, Budapest, Hungary

M. Csand , K. Farkas , A. Fehrkuti³³ , M.M.A. Gadallah³⁴ , . Kadlecik , P. Major , G. Pasztor , G.I. Veres 

Faculty of Informatics, University of Debrecen, Debrecen, Hungary

B. Ujvari , G. Zilizi 

Institute of Nuclear Research ATOMKI, Debrecen, Hungary

G. Bencze, S. Czellar, J. Molnar, Z. Szillasi

Karoly Robert Campus, MATE Institute of Technology, Gyongyos, Hungary

F. Nemes³³ , T. Novak 

Panjab University, Chandigarh, India

J. Babbar , S. Bansal , S.B. Beri, V. Bhatnagar , G. Chaudhary , S. Chauhan , N. Dhingra³⁵ , A. Kaur , A. Kaur , H. Kaur , M. Kaur , S. Kumar , K. Sandeep , T. Sheokand, J.B. Singh , A. Singla

University of Delhi, Delhi, India

A. Ahmed , A. Bhardwaj , A. Chhetri , B.C. Choudhary , A. Kumar , A. Kumar , M. Naimuddin , K. Ranjan , M.K. Saini, S. Saumya

Saha Institute of Nuclear Physics, HBNI, Kolkata, India

S. Baradia , S. Barman³⁶ , S. Bhattacharya , S. Das Gupta, S. Dutta , S. Dutta, S. Sarkar

Indian Institute of Technology Madras, Madras, India

M.M. Ameen , P.K. Behera , S.C. Behera , S. Chatterjee , G. Dash , P. Jana , P. Kalbhor , S. Kamble , J.R. Komaragiri³⁷ , D. Kumar³⁷ , P.R. Pujahari , N.R. Saha , A. Sharma , A.K. Sikdar , R.K. Singh, P. Verma, S. Verma , A. Vijay

Tata Institute of Fundamental Research-A, Mumbai, IndiaS. Dugad, G.B. Mohanty , B. Parida , M. Shelake, P. Suryadevara**Tata Institute of Fundamental Research-B, Mumbai, India**A. Bala , S. Banerjee , R.M. Chatterjee, M. Guchait , Sh. Jain , A. Jaiswal, S. Kumar , G. Majumder , K. Mazumdar , S. Parolia , A. Thachayath **National Institute of Science Education and Research, An OCC of Homi Bhabha National Institute, Bhubaneswar, Odisha, India**S. Bahinipati³⁸ , C. Kar , D. Maity³⁹ , P. Mal , T. Mishra , V.K. Muraleedharan Nair Bindhu³⁹ , K. Naskar³⁹ , A. Nayak³⁹ , S. Nayak, K. Pal, P. Sadangi, S.K. Swain , S. Varghese³⁹ , D. Vats³⁹ **Indian Institute of Science Education and Research (IISER), Pune, India**S. Acharya⁴⁰ , A. Alpana , S. Dube , B. Gomber⁴⁰ , P. Hazarika , B. Kansal , A. Laha , B. Sahu⁴⁰ , S. Sharma , K.Y. Vaish **Isfahan University of Technology, Isfahan, Iran**H. Bakhshiansohi⁴¹ , A. Jafari⁴² , M. Zeinali⁴³ **Institute for Research in Fundamental Sciences (IPM), Tehran, Iran**S. Bashiri, S. Chenarani⁴⁴ , S.M. Etesami , Y. Hosseini , M. Khakzad , E. Khazaie⁴⁵ , M. Mohammadi Najafabadi , S. Tizchang⁴⁶ **University College Dublin, Dublin, Ireland**M. Felcini , M. Grunewald **INFN Sezione di Bari^a, Università di Bari^b, Politecnico di Bari^c, Bari, Italy**M. Abbrescia^{a,b} , A. Colaleo^{a,b} , D. Creanza^{a,c} , B. D'Anzi^{a,b} , N. De Filippis^{a,c} , M. De Palma^{a,b} , W. Elmetenawee^{a,b,47} , L. Fiore^a , G. Iaselli^{a,c} , L. Longo^a , M. Louka^{a,b} , G. Maggi^{a,c} , M. Maggi^a , I. Margjeka^a , V. Mastrapasqua^{a,b} , S. My^{a,b} , S. Nuzzo^{a,b} , A. Pellecchia^{a,b} , A. Pompili^{a,b} , G. Pugliese^{a,c} , R. Radogna^{a,b} , D. Ramos^a , A. Ranieri^a , L. Silvestris^a , F.M. Simone^{a,c} , Ü. Sözbilir^a , A. Stamerra^{a,b} , D. Troiano^{a,b} , R. Venditti^{a,b} , P. Verwilligen^a , A. Zaza^{a,b} **INFN Sezione di Bologna^a, Università di Bologna^b, Bologna, Italy**G. Abbiendi^a , C. Battilana^{a,b} , D. Bonacorsi^{a,b} , P. Capiluppi^{a,b} , A. Castro^{+a,b} , F.R. Cavallo^a , M. Cuffiani^{a,b} , G.M. Dallavalle^a , T. Diotalevi^{a,b} , F. Fabbri^a , A. Fanfani^{a,b} , D. Fasanella^a , P. Giacomelli^a , L. Giommi^{a,b} , C. Grandi^a , L. Guiducci^{a,b} , S. Lo Meo^{a,48} , M. Lorusso^{a,b} , L. Lunerti^a , S. Marcellini^a , G. Masetti^a , F.L. Navarria^{a,b} , G. Paggi^{a,b} , A. Perrotta^a , F. Primavera^{a,b} , A.M. Rossi^{a,b} , S. Rossi Tisbeni^{a,b} , T. Rovelli^{a,b} , G.P. Siroli^{a,b} **INFN Sezione di Catania^a, Università di Catania^b, Catania, Italy**S. Costa^{a,b,49} , A. Di Mattia^a , A. Lapertosa^a , R. Potenza^{a,b}, A. Tricomi^{a,b,49} , C. Tuve^{a,b} **INFN Sezione di Firenze^a, Università di Firenze^b, Firenze, Italy**P. Assiouras^a , G. Barbagli^a , G. Bardelli^{a,b} , B. Camaiani^{a,b} , A. Cassese^a , R. Ceccarelli^a , V. Ciulli^{a,b} , C. Civinini^a , R. D'Alessandro^{a,b} , E. Focardi^{a,b} , T. Kello^a, G. Latino^{a,b} , P. Lenzi^{a,b} , M. Lizzo^a , M. Meschini^a , S. Paoletti^a , A. Papanastassiou^{a,b} , G. Sguazzoni^a , L. Viliani^a **INFN Laboratori Nazionali di Frascati, Frascati, Italy**L. Benussi , S. Bianco , S. Meola⁵⁰ , D. Piccolo 

INFN Sezione di Genova^a, Università di Genova^b, Genova, Italy

P. Chatagnon^a , F. Ferro^a , E. Robutti^a , S. Tosi^{a,b} 

INFN Sezione di Milano-Bicocca^a, Università di Milano-Bicocca^b, Milano, Italy

A. Benaglia^a , F. Brivio^a , F. Cetorelli^{a,b} , F. De Guio^{a,b} , M.E. Dinardo^{a,b} , P. Dini^a , S. Gennai^a , R. Gerosa^{a,b} , A. Ghezzi^{a,b} , P. Govoni^{a,b} , L. Guzzi^a , M.T. Lucchini^{a,b} , M. Malberti^a , S. Malvezzi^a , A. Massironi^a , D. Menasce^a , L. Moroni^a , M. Paganoni^{a,b} , S. Pallotto^{a,b} , D. Pedrini^a , A. Perego^{a,b} , B.S. Pinolini^a, G. Pizzati^{a,b} , S. Ragazzi^{a,b} , T. Tabarelli de Fatis^{a,b} 

INFN Sezione di Napoli^a, Università di Napoli 'Federico II'^b, Napoli, Italy; Università della Basilicata^c, Potenza, Italy; Scuola Superiore Meridionale (SSM)^d, Napoli, Italy

S. Buontempo^a , A. Cagnotta^{a,b} , F. Carnevali^{a,b} , N. Cavallo^{a,c} , F. Fabozzi^{a,c} , A.O.M. Iorio^{a,b} , L. Lista^{a,b,51} , P. Paoluccia^{a,29} 

INFN Sezione di Padova^a, Università di Padova^b, Padova, Italy; Università di Trento^c, Trento, Italy

R. Ardino^a , P. Azzi^a , N. Bacchetta^{a,52} , D. Bisello^{a,b} , P. Bortignon^a , G. Bortolato^{a,b} , A. Bragagnolo^{a,b} , A.C.M. Bulla^a , R. Carlin^{a,b} , P. Checchia^a , T. Dorigo^a , F. Gasparini^{a,b} , U. Gasparini^{a,b} , E. Lusiani^a , M. Margoni^{a,b} , A.T. Meneguzzo^{a,b} , M. Migliorini^{a,b} , M. Passaseo^a , J. Pazzini^{a,b} , P. Ronchese^{a,b} , R. Rossin^{a,b} , M. Tosi^{a,b} , A. Triossi^{a,b} , S. Ventura^a , M. Zanetti^{a,b} , P. Zotto^{a,b} , A. Zucchetta^{a,b} , G. Zumerle^{a,b} 

INFN Sezione di Pavia^a, Università di Pavia^b, Pavia, Italy

C. Aimè^a , A. Braghieri^a , S. Calzaferri^a , D. Fiorina^a , P. Montagna^{a,b} , V. Re^a , C. Riccardi^{a,b} , P. Salvini^a , I. Vai^{a,b} , P. Vitulo^{a,b} 

INFN Sezione di Perugia^a, Università di Perugia^b, Perugia, Italy

S. Ajmal^{a,b} , M.E. Ascoli^{a,b} , G.M. Bilei^a , C. Carrivale^{a,b} , D. Ciangottini^{a,b} , L. Fanò^{a,b} , M. Magherini^{a,b} , V. Mariani^{a,b} , M. Menichelli^a , F. Moscatelli^{a,53} , A. Rossi^{a,b} , A. Santocchia^{a,b} , D. Spiga^a , T. Tedeschi^{a,b} 

INFN Sezione di Pisa^a, Università di Pisa^b, Scuola Normale Superiore di Pisa^c, Pisa, Italy; Università di Siena^d, Siena, Italy

C.A. Alexe^{a,c} , P. Asenov^{a,b} , P. Azzurri^a , G. Bagliesi^a , R. Bhattacharya^a , L. Bianchini^{a,b} , T. Boccali^a , E. Bossini^a , D. Bruschini^{a,c} , R. Castaldi^a , M.A. Ciocci^{a,b} , M. Cipriani^{a,b} , V. D'Amante^{a,d} , R. Dell'Orso^a , S. Donato^a , A. Giassi^a , F. Ligabue^{a,c} , A.C. Marini^a , D. Matos Figueiredo^a , A. Messineo^{a,b} , M. Musich^{a,b} , F. Palla^a , A. Rizzi^{a,b} , G. Rolandi^{a,c} , S. Roy Chowdhury^a , T. Sarkar^a , A. Scribano^a , P. Spagnolo^a , R. Tenchini^a , G. Tonelli^{a,b} , N. Turini^{a,d} , F. Vaselli^{a,c} , A. Venturi^a , P.G. Verdini^a 

INFN Sezione di Roma^a, Sapienza Università di Roma^b, Roma, Italy

C. Baldenegro Barrera^{a,b} , P. Barria^a , C. Basile^{a,b} , M. Campana^{a,b} , F. Cavallari^a , L. Cunqueiro Mendez^{a,b} , D. Del Re^{a,b} , E. Di Marco^{a,b} , M. Diemoz^a , F. Errico^{a,b} , E. Longo^{a,b} , J. Mijuskovic^{a,b} , G. Organtini^{a,b} , F. Pandolfi^a , R. Paramatti^{a,b} , C. Quaranta^{a,b} , S. Rahatlou^{a,b} , C. Rovelli^a , F. Santanastasio^{a,b} , L. Soffi^a 

INFN Sezione di Torino^a, Università di Torino^b, Torino, Italy; Università del Piemonte Orientale^c, Novara, Italy

N. Amapane^{a,b} , R. Arcidiacono^{a,c} , S. Argiro^{a,b} , M. Arneodo^{a,c} , N. Bartosik^a , R. Bellan^{a,b} , A. Bellora^{a,b} , C. Biino^a , C. Borca^{a,b} , N. Cartiglia^a , M. Costa^{a,b} 

R. Covarelli^{a,b} , N. Demaria^a , L. Finco^a , M. Grippo^{a,b} , B. Kiani^{a,b} , F. Legger^a , F. Luongo^{a,b} , C. Mariotti^a , L. Markovic^{a,b} , S. Maselli^a , A. Mecca^{a,b} , L. Menzio^{a,b} , P. Meridiani^a , E. Migliore^{a,b} , M. Monteno^a , R. Mulargia^a , M.M. Obertino^{a,b} , G. Ortona^a , L. Pacher^{a,b} , N. Pastrone^a , M. Pelliccioni^a , M. Ruspa^{a,c} , F. Siviero^{a,b} , V. Sola^{a,b} , A. Solano^{a,b} , A. Staiano^a , C. Tarricone^{a,b} , D. Trocino^a , G. Umoret^{a,b} , R. White^{a,b}

INFN Sezione di Trieste^a, Università di Trieste^b, Trieste, Italy

S. Belforte^a , V. Candeliere^{a,b} , M. Casarsa^a , F. Cossutti^a , K. De Leo^a , G. Della Ricca^{a,b} 

Kyungpook National University, Daegu, Korea

S. Dogra , J. Hong , C. Huh , B. Kim , J. Kim, D. Lee, H. Lee, S.W. Lee , C.S. Moon , Y.D. Oh , M.S. Ryu , S. Sekmen , B. Tae, Y.C. Yang

Department of Mathematics and Physics - GWNU, Gangneung, Korea

M.S. Kim 

Chonnam National University, Institute for Universe and Elementary Particles, Kwangju, Korea

G. Bak , P. Gwak , H. Kim , D.H. Moon 

Hanyang University, Seoul, Korea

E. Asilar , J. Choi , D. Kim , T.J. Kim , J.A. Merlin, Y. Ryou

Korea University, Seoul, Korea

S. Choi , S. Han, B. Hong , K. Lee, K.S. Lee , S. Lee , J. Yoo 

Kyung Hee University, Department of Physics, Seoul, Korea

J. Goh , S. Yang 

Sejong University, Seoul, Korea

H. S. Kim , Y. Kim, S. Lee

Seoul National University, Seoul, Korea

J. Almond, J.H. Bhyun, J. Choi , J. Choi, W. Jun , J. Kim , S. Ko , H. Kwon , H. Lee , J. Lee , J. Lee , B.H. Oh , S.B. Oh , H. Seo , U.K. Yang, I. Yoon

University of Seoul, Seoul, Korea

W. Jang , D.Y. Kang, Y. Kang , S. Kim , B. Ko, J.S.H. Lee , Y. Lee , I.C. Park , Y. Roh, I.J. Watson 

Yonsei University, Department of Physics, Seoul, Korea

S. Ha , H.D. Yoo 

Sungkyunkwan University, Suwon, Korea

M. Choi , M.R. Kim , H. Lee, Y. Lee , I. Yu 

College of Engineering and Technology, American University of the Middle East (AUM), Dasman, Kuwait

T. Beyrouty, Y. Gharbia

Kuwait University - College of Science - Department of Physics, Safat, Kuwait

F. Alazemi 

Riga Technical University, Riga, Latvia

K. Dreimanis , A. Gaile , G. Pikurs, A. Potrebko , M. Seidel , D. Sidiropoulos Kontos

University of Latvia (LU), Riga, LatviaN.R. Strautnieks **Vilnius University, Vilnius, Lithuania**M. Ambrozas , A. Juodagalvis , A. Rinkevicius , G. Tamulaitis **National Centre for Particle Physics, Universiti Malaya, Kuala Lumpur, Malaysia**I. Yusuff⁵⁴ , Z. Zolkapli**Universidad de Sonora (UNISON), Hermosillo, Mexico**J.F. Benitez , A. Castaneda Hernandez , H.A. Encinas Acosta, L.G. Gallegos Maríñez, M. León Coello , J.A. Murillo Quijada , A. Sehrawat , L. Valencia Palomo **Centro de Investigacion y de Estudios Avanzados del IPN, Mexico City, Mexico**G. Ayala , H. Castilla-Valdez , H. Crotte Ledesma, E. De La Cruz-Burelo , I. Heredia-De La Cruz⁵⁵ , R. Lopez-Fernandez , J. Mejia Guisao , C.A. Mondragon Herrera, A. Sánchez Hernández **Universidad Iberoamericana, Mexico City, Mexico**C. Oropeza Barrera , D.L. Ramirez Guadarrama, M. Ramírez García **Benemerita Universidad Autonoma de Puebla, Puebla, Mexico**I. Bautista , I. Pedraza , H.A. Salazar Ibarguen , C. Uribe Estrada **University of Montenegro, Podgorica, Montenegro**I. Bubanja , N. Raicevic **University of Canterbury, Christchurch, New Zealand**P.H. Butler **National Centre for Physics, Quaid-I-Azam University, Islamabad, Pakistan**A. Ahmad , M.I. Asghar, A. Awais , M.I.M. Awan, H.R. Hoorani , W.A. Khan **AGH University of Krakow, Faculty of Computer Science, Electronics and Telecommunications, Krakow, Poland**V. Avati, L. Grzanka , M. Malawski **National Centre for Nuclear Research, Swierk, Poland**H. Bialkowska , M. Bluj , M. Górski , M. Kazana , M. Szleper , P. Zalewski **Institute of Experimental Physics, Faculty of Physics, University of Warsaw, Warsaw, Poland**K. Bunkowski , K. Doroba , A. Kalinowski , M. Konecki , J. Krolikowski , A. Muhammad **Warsaw University of Technology, Warsaw, Poland**K. Pozniak , W. Zabolotny **Laboratório de Instrumentação e Física Experimental de Partículas, Lisboa, Portugal**M. Araujo , D. Bastos , C. Beirão Da Cruz E Silva , A. Boletti , M. Bozzo , T. Camporesi , G. Da Molin , M. Gallinaro , J. Hollar , N. Leonardo , G.B. Marozzo, T. Niknejad , A. Petrilli , M. Pisano , J. Seixas , J. Varela , J.W. Wulff**Faculty of Physics, University of Belgrade, Belgrade, Serbia**P. Adzic , P. Milenovic **VINCA Institute of Nuclear Sciences, University of Belgrade, Belgrade, Serbia**M. Dordevic , J. Milosevic , V. Rekovic

Centro de Investigaciones Energéticas Medioambientales y Tecnológicas (CIEMAT), Madrid, Spain

J. Alcaraz Maestre [ID](#), Cristina F. Bedoya [ID](#), Oliver M. Carretero [ID](#), M. Cepeda [ID](#), M. Cerrada [ID](#), N. Colino [ID](#), B. De La Cruz [ID](#), A. Delgado Peris [ID](#), A. Escalante Del Valle [ID](#), D. Fernández Del Val [ID](#), J.P. Fernández Ramos [ID](#), J. Flix [ID](#), M.C. Fouz [ID](#), O. Gonzalez Lopez [ID](#), S. Goy Lopez [ID](#), J.M. Hernandez [ID](#), M.I. Josa [ID](#), E. Martin Viscasillas [ID](#), D. Moran [ID](#), C. M. Morcillo Perez [ID](#), Á. Navarro Tobar [ID](#), C. Perez Dengra [ID](#), A. Pérez-Calero Yzquierdo [ID](#), J. Puerta Pelayo [ID](#), I. Redondo [ID](#), S. Sánchez Navas [ID](#), J. Sastre [ID](#), J. Vazquez Escobar [ID](#)

Universidad Autónoma de Madrid, Madrid, Spain

J.F. de Trocóniz [ID](#)

Universidad de Oviedo, Instituto Universitario de Ciencias y Tecnologías Espaciales de Asturias (ICTEA), Oviedo, Spain

B. Alvarez Gonzalez [ID](#), J. Cuevas [ID](#), J. Fernandez Menendez [ID](#), S. Folgueras [ID](#), I. Gonzalez Caballero [ID](#), J.R. González Fernández [ID](#), P. Leguina [ID](#), E. Palencia Cortezon [ID](#), J. Prado Pico, C. Ramón Alvarez [ID](#), V. Rodríguez Bouza [ID](#), A. Soto Rodríguez [ID](#), A. Trapote [ID](#), C. Vico Villalba [ID](#), P. Vischia [ID](#)

Instituto de Física de Cantabria (IFCA), CSIC-Universidad de Cantabria, Santander, Spain

S. Bhowmik [ID](#), S. Blanco Fernández [ID](#), J.A. Brochero Cifuentes [ID](#), I.J. Cabrillo [ID](#), A. Calderon [ID](#), J. Duarte Campderros [ID](#), M. Fernandez [ID](#), G. Gomez [ID](#), C. Lasosa García [ID](#), R. Lopez Ruiz [ID](#), C. Martinez Rivero [ID](#), P. Martinez Ruiz del Arbol [ID](#), F. Matorras [ID](#), P. Matorras Cuevas [ID](#), E. Navarrete Ramos [ID](#), J. Piedra Gomez [ID](#), L. Scodellaro [ID](#), I. Vila [ID](#), J.M. Vizan Garcia [ID](#)

University of Colombo, Colombo, Sri Lanka

B. Kailasapathy⁵⁶ [ID](#), D.D.C. Wickramarathna [ID](#)

University of Ruhuna, Department of Physics, Matara, Sri Lanka

W.G.D. Dharmaratna⁵⁷ [ID](#), K. Liyanage [ID](#), N. Perera [ID](#)

CERN, European Organization for Nuclear Research, Geneva, Switzerland

D. Abbaneo [ID](#), C. Amendola [ID](#), E. Auffray [ID](#), G. Auzinger [ID](#), J. Baechler, D. Barney [ID](#), A. Bermúdez Martínez [ID](#), M. Bianco [ID](#), A.A. Bin Anuar [ID](#), A. Bocci [ID](#), L. Borgonovi [ID](#), C. Botta [ID](#), E. Brondolin [ID](#), C. Caillol [ID](#), G. Cerminara [ID](#), N. Chernyavskaya [ID](#), D. d'Enterria [ID](#), A. Dabrowski [ID](#), A. David [ID](#), A. De Roeck [ID](#), M.M. Defranchis [ID](#), M. Deile [ID](#), M. Dobson [ID](#), G. Franzoni [ID](#), W. Funk [ID](#), S. Giani, D. Gigi, K. Gill [ID](#), F. Glege [ID](#), J. Hegeman [ID](#), J.K. Heikkilä [ID](#), B. Huber, V. Innocente [ID](#), T. James [ID](#), P. Janot [ID](#), O. Kaluzinska [ID](#), O. Karacheban²⁷ [ID](#), S. Laurila [ID](#), P. Lecoq [ID](#), E. Leutgeb [ID](#), C. Lourenço [ID](#), L. Malgeri [ID](#), M. Mannelli [ID](#), M. Matthewman, A. Mehta [ID](#), F. Meijers [ID](#), S. Mersi [ID](#), E. Meschi [ID](#), V. Milosevic [ID](#), F. Monti [ID](#), F. Moortgat [ID](#), M. Mulders [ID](#), I. Neutelings [ID](#), S. Orfanelli, F. Pantaleo [ID](#), G. Petrucciani [ID](#), A. Pfeiffer [ID](#), M. Pierini [ID](#), H. Qu [ID](#), D. Rabady [ID](#), B. Ribeiro Lopes [ID](#), M. Rovere [ID](#), H. Sakulin [ID](#), S. Sanchez Cruz [ID](#), S. Scarfi [ID](#), C. Schwick, M. Selvaggi [ID](#), A. Sharma [ID](#), K. Shchelina [ID](#), P. Silva [ID](#), P. Sphicas⁵⁸ [ID](#), A.G. Stahl Leiton [ID](#), A. Steen [ID](#), S. Summers [ID](#), D. Treille [ID](#), P. Tropea [ID](#), D. Walter [ID](#), J. Wanczyk⁵⁹ [ID](#), J. Wang, S. Wuchterl [ID](#), P. Zehetner [ID](#), P. Zejdl [ID](#), W.D. Zeuner

Paul Scherrer Institut, Villigen, Switzerland

T. Bevilacqua⁶⁰ [ID](#), L. Caminada⁶⁰ [ID](#), A. Ebrahimi [ID](#), W. Erdmann [ID](#), R. Horisberger [ID](#), Q. Ingram [ID](#), H.C. Kaestli [ID](#), D. Kotlinski [ID](#), C. Lange [ID](#), M. Missiroli⁶⁰ [ID](#), L. Noehte⁶⁰ [ID](#), T. Rohe [ID](#)

ETH Zurich - Institute for Particle Physics and Astrophysics (IPA), Zurich, Switzerland

T.K. Aarrestad , K. Androssov⁵⁹ , M. Backhaus , G. Bonomelli, A. Calandri , C. Cazzaniga , K. Datta , P. De Bryas Dexmiers D'archiac⁵⁹ , A. De Cosa , G. Dissertori , M. Dittmar, M. Donegà , F. Eble , M. Galli , K. Gedia , F. Glessgen , C. Grab , N. Härringer , T.G. Harte, D. Hits , W. Lustermann , A.-M. Lyon , R.A. Manzoni , M. Marchegiani , L. Marchese , C. Martin Perez , A. Mascellani⁵⁹ , F. Nessi-Tedaldi , F. Pauss , V. Perovic , S. Pigazzini , C. Reissel , B. Ristic , F. Riti , R. Seidita , J. Steggemann⁵⁹ , A. Tarabini , D. Valsecchi , R. Wallny

Universität Zürich, Zurich, Switzerland

C. Amsler⁶¹ , P. Bärtschi , M.F. Canelli , K. Cormier , M. Huwiler , W. Jin , A. Jofrehei , B. Kilminster , S. Leontsinis , S.P. Liechti , A. Macchiolo , P. Meiring , F. Meng , U. Molinatti , J. Motta , A. Reimers , P. Robmann, M. Senger , E. Shokr, F. Stäger , R. Tramontano

National Central University, Chung-Li, Taiwan

C. Adloff⁶², D. Bhowmik, C.M. Kuo, W. Lin, P.K. Rout , P.C. Tiwari³⁷ , S.S. Yu 

National Taiwan University (NTU), Taipei, Taiwan

L. Ceard, K.F. Chen , P.s. Chen, Z.g. Chen, A. De Iorio , W.-S. Hou , T.h. Hsu, Y.w. Kao, S. Karmakar , G. Kole , Y.y. Li , R.-S. Lu , E. Paganis , X.f. Su , J. Thomas-Wilsker , L.s. Tsai, D. Tsionou, H.y. Wu, E. Yazgan

High Energy Physics Research Unit, Department of Physics, Faculty of Science, Chulalongkorn University, Bangkok, Thailand

C. Asawatangtrakuldee , N. Srimanobhas , V. Wachirapusanand 

Çukurova University, Physics Department, Science and Art Faculty, Adana, Turkey

D. Agyel , F. Boran , F. Dolek , I. Dumanoglu⁶³ , E. Eskut , Y. Guler⁶⁴ , E. Gurpinar Guler⁶⁴ , C. Isik , O. Kara, A. Kayis Topaksu , U. Kiminsu , G. Onengut , K. Ozdemir⁶⁵ , A. Polatoz , B. Tali⁶⁶ , U.G. Tok , S. Turkcapar , E. Uslan , I.S. Zorbakir

Middle East Technical University, Physics Department, Ankara, Turkey

G. Sokmen, M. Yalvac⁶⁷ 

Bogazici University, Istanbul, Turkey

B. Akgun , I.O. Atakisi , E. Gülmез , M. Kaya⁶⁸ , O. Kaya⁶⁹ , S. Tekten⁷⁰ 

Istanbul Technical University, Istanbul, Turkey

A. Cakir , K. Cankocak^{63,71} , G.G. Dincer⁶³ , Y. Komurcu , S. Sen⁷² 

Istanbul University, Istanbul, Turkey

O. Aydilek⁷³ , B. Hacisahinoglu , I. Hos⁷⁴ , B. Kaynak , S. Ozkorucuklu , O. Potok , H. Sert , C. Simsek , C. Zorbilmez

Yildiz Technical University, Istanbul, Turkey

S. Cerci⁶⁶ , B. Isildak⁷⁵ , D. Sunar Cerci , T. Yetkin 

Institute for Scintillation Materials of National Academy of Science of Ukraine, Kharkiv, Ukraine

A. Boyaryntsev , B. Grynyov 

National Science Centre, Kharkiv Institute of Physics and Technology, Kharkiv, Ukraine

L. Levchuk 

University of Bristol, Bristol, United Kingdom

D. Anthony [ID](#), J.J. Brooke [ID](#), A. Bundock [ID](#), F. Bury [ID](#), E. Clement [ID](#), D. Cussans [ID](#), H. Flacher [ID](#), M. Glowacki, J. Goldstein [ID](#), H.F. Heath [ID](#), M.-L. Holmberg [ID](#), L. Kreczko [ID](#), S. Paramesvaran [ID](#), L. Robertshaw, S. Seif El Nasr-Storey, V.J. Smith [ID](#), N. Stylianou⁷⁶ [ID](#), K. Walkingshaw Pass

Rutherford Appleton Laboratory, Didcot, United Kingdom

A.H. Ball, K.W. Bell [ID](#), A. Belyaev⁷⁷ [ID](#), C. Brew [ID](#), R.M. Brown [ID](#), D.J.A. Cockerill [ID](#), C. Cooke [ID](#), A. Elliot [ID](#), K.V. Ellis, K. Harder [ID](#), S. Harper [ID](#), J. Linacre [ID](#), K. Manolopoulos, D.M. Newbold [ID](#), E. Olaiya, D. Petyt [ID](#), T. Reis [ID](#), A.R. Sahasransu [ID](#), G. Salvi [ID](#), T. Schuh, C.H. Shepherd-Themistocleous [ID](#), I.R. Tomalin [ID](#), K.C. Whalen [ID](#), T. Williams [ID](#)

Imperial College, London, United Kingdom

I. Andreou [ID](#), R. Bainbridge [ID](#), P. Bloch [ID](#), C.E. Brown [ID](#), O. Buchmuller, V. Cacchio, C.A. Carrillo Montoya [ID](#), G.S. Chahal⁷⁸ [ID](#), D. Colling [ID](#), J.S. Dancu, I. Das [ID](#), P. Dauncey [ID](#), G. Davies [ID](#), J. Davies, M. Della Negra [ID](#), S. Fayer, G. Fedi [ID](#), G. Hall [ID](#), M.H. Hassanshahi [ID](#), A. Howard, G. Iles [ID](#), M. Knight [ID](#), J. Langford [ID](#), J. León Holgado [ID](#), L. Lyons [ID](#), A.-M. Magnan [ID](#), S. Mallios, M. Mieskolainen [ID](#), J. Nash⁷⁹ [ID](#), M. Pesaresi [ID](#), P.B. Pradeep, B.C. Radburn-Smith [ID](#), A. Richards, A. Rose [ID](#), K. Savva [ID](#), C. Seez [ID](#), R. Shukla [ID](#), A. Tapper [ID](#), K. Uchida [ID](#), G.P. Uttley [ID](#), L.H. Vage, T. Virdee²⁹ [ID](#), M. Vojinovic [ID](#), N. Wardle [ID](#), D. Winterbottom [ID](#)

Brunel University, Uxbridge, United Kingdom

K. Coldham, J.E. Cole [ID](#), A. Khan, P. Kyberd [ID](#), I.D. Reid [ID](#)

Baylor University, Waco, Texas, USA

S. Abdullin [ID](#), A. Brinkerhoff [ID](#), E. Collins [ID](#), J. Dittmann [ID](#), K. Hatakeyama [ID](#), J. Hiltbrand [ID](#), B. McMaster [ID](#), J. Samudio [ID](#), S. Sawant [ID](#), C. Sutantawibul [ID](#), J. Wilson [ID](#)

Catholic University of America, Washington, DC, USA

R. Bartek [ID](#), A. Dominguez [ID](#), C. Huerta Escamilla, A.E. Simsek [ID](#), R. Uniyal [ID](#), A.M. Vargas Hernandez [ID](#)

The University of Alabama, Tuscaloosa, Alabama, USA

B. Bam [ID](#), A. Buchot Perraguin [ID](#), R. Chudasama [ID](#), S.I. Cooper [ID](#), C. Crovella [ID](#), S.V. Gleyzer [ID](#), E. Pearson, C.U. Perez [ID](#), P. Rumerio⁸⁰ [ID](#), E. Usai [ID](#), R. Yi [ID](#)

Boston University, Boston, Massachusetts, USA

A. Akpinar [ID](#), C. Cosby [ID](#), G. De Castro, Z. Demiragli [ID](#), C. Erice [ID](#), C. Fangmeier [ID](#), C. Fernandez Madrazo [ID](#), E. Fontanesi [ID](#), D. Gastler [ID](#), F. Golf [ID](#), S. Jeon [ID](#), J. O'cain, I. Reed [ID](#), J. Rohlf [ID](#), K. Salyer [ID](#), D. Sperka [ID](#), D. Spitzbart [ID](#), I. Suarez [ID](#), A. Tsatsos [ID](#), A.G. Zecchinelli [ID](#)

Brown University, Providence, Rhode Island, USA

G. Benelli [ID](#), D. Cutts [ID](#), L. Gouskos [ID](#), M. Hadley [ID](#), U. Heintz [ID](#), J.M. Hogan⁸¹ [ID](#), T. Kwon [ID](#), G. Landsberg [ID](#), K.T. Lau [ID](#), D. Li [ID](#), J. Luo [ID](#), S. Mondal [ID](#), N. Pervan [ID](#), T. Russell, S. Sagir⁸² [ID](#), F. Simpson [ID](#), M. Stamenkovic [ID](#), N. Venkatasubramanian, X. Yan [ID](#)

University of California, Davis, Davis, California, USA

S. Abbott [ID](#), C. Brainerd [ID](#), R. Breedon [ID](#), H. Cai [ID](#), M. Calderon De La Barca Sanchez [ID](#), M. Chertok [ID](#), M. Citron [ID](#), J. Conway [ID](#), P.T. Cox [ID](#), R. Erbacher [ID](#), F. Jensen [ID](#), O. Kukral [ID](#), G. Mocellin [ID](#), M. Mulhearn [ID](#), S. Ostrom [ID](#), W. Wei [ID](#), Y. Yao [ID](#), S. Yoo [ID](#), F. Zhang [ID](#)

University of California, Los Angeles, California, USA

M. Bachtis [ID](#), R. Cousins [ID](#), A. Datta [ID](#), G. Flores Avila [ID](#), J. Hauser [ID](#), M. Ignatenko [ID](#), M.A. Iqbal [ID](#), T. Lam [ID](#), E. Manca [ID](#), A. Nunez Del Prado, D. Saltzberg [ID](#), V. Valuev [ID](#)

University of California, Riverside, Riverside, California, USA

R. Clare [ID](#), J.W. Gary [ID](#), M. Gordon, G. Hanson [ID](#), W. Si [ID](#)

University of California, San Diego, La Jolla, California, USA

A. Aportela, A. Arora [ID](#), J.G. Branson [ID](#), S. Cittolin [ID](#), S. Cooperstein [ID](#), D. Diaz [ID](#), J. Duarte [ID](#), L. Giannini [ID](#), Y. Gu, J. Guiang [ID](#), R. Kansal [ID](#), V. Krutelyov [ID](#), R. Lee [ID](#), J. Letts [ID](#), M. Masciovecchio [ID](#), F. Mokhtar [ID](#), S. Mukherjee [ID](#), M. Pieri [ID](#), M. Quinnan [ID](#), B.V. Sathia Narayanan [ID](#), V. Sharma [ID](#), M. Tadel [ID](#), E. Vourliotis [ID](#), F. Würthwein [ID](#), Y. Xiang [ID](#), A. Yagil [ID](#)

University of California, Santa Barbara - Department of Physics, Santa Barbara, California, USA

A. Barzdukas [ID](#), L. Brennan [ID](#), C. Campagnari [ID](#), K. Downham [ID](#), C. Grieco [ID](#), J. Incandela [ID](#), J. Kim [ID](#), A.J. Li [ID](#), P. Masterson [ID](#), H. Mei [ID](#), J. Richman [ID](#), S.N. Santpur [ID](#), U. Sarica [ID](#), R. Schmitz [ID](#), F. Setti [ID](#), J. Sheplock [ID](#), D. Stuart [ID](#), T.Á. Vámi [ID](#), S. Wang [ID](#), D. Zhang

California Institute of Technology, Pasadena, California, USA

A. Bornheim [ID](#), O. Cerri, A. Latorre, J. Mao [ID](#), H.B. Newman [ID](#), G. Reales Gutiérrez, M. Spiropulu [ID](#), J.R. Vlimant [ID](#), C. Wang [ID](#), S. Xie [ID](#), R.Y. Zhu [ID](#)

Carnegie Mellon University, Pittsburgh, Pennsylvania, USA

J. Alison [ID](#), S. An [ID](#), P. Bryant [ID](#), M. Cremonesi, V. Dutta [ID](#), T. Ferguson [ID](#), T.A. Gómez Espinosa [ID](#), A. Harilal [ID](#), A. Kallil Tharayil, C. Liu [ID](#), T. Mudholkar [ID](#), S. Murthy [ID](#), P. Palit [ID](#), K. Park, M. Paulini [ID](#), A. Roberts [ID](#), A. Sanchez [ID](#), W. Terrill [ID](#)

University of Colorado Boulder, Boulder, Colorado, USA

J.P. Cumalat [ID](#), W.T. Ford [ID](#), A. Hart [ID](#), A. Hassani [ID](#), G. Karathanasis [ID](#), N. Manganelli [ID](#), C. Savard [ID](#), N. Schonbeck [ID](#), K. Stenson [ID](#), K.A. Ulmer [ID](#), S.R. Wagner [ID](#), N. Zipper [ID](#), D. Zuolo [ID](#)

Cornell University, Ithaca, New York, USA

J. Alexander [ID](#), S. Bright-Thonney [ID](#), X. Chen [ID](#), D.J. Cranshaw [ID](#), J. Fan [ID](#), X. Fan [ID](#), S. Hogan [ID](#), P. Kotamnives, J. Monroy [ID](#), M. Oshiro [ID](#), J.R. Patterson [ID](#), M. Reid [ID](#), A. Ryd [ID](#), J. Thom [ID](#), P. Wittich [ID](#), R. Zou [ID](#)

Fermi National Accelerator Laboratory, Batavia, Illinois, USA

M. Albrow [ID](#), M. Alyari [ID](#), O. Amram [ID](#), G. Apollinari [ID](#), A. Apresyan [ID](#), L.A.T. Bauerdick [ID](#), D. Berry [ID](#), J. Berryhill [ID](#), P.C. Bhat [ID](#), K. Burkett [ID](#), J.N. Butler [ID](#), A. Canepa [ID](#), G.B. Cerati [ID](#), H.W.K. Cheung [ID](#), F. Chlebana [ID](#), G. Cummings [ID](#), J. Dickinson [ID](#), I. Dutta [ID](#), V.D. Elvira [ID](#), Y. Feng [ID](#), J. Freeman [ID](#), A. Gandrakota [ID](#), Z. Gecse [ID](#), L. Gray [ID](#), D. Green, A. Grummer [ID](#), S. Grünendahl [ID](#), D. Guerrero [ID](#), O. Gutsche [ID](#), R.M. Harris [ID](#), R. Heller [ID](#), T.C. Herwig [ID](#), J. Hirschauer [ID](#), B. Jayatilaka [ID](#), S. Jindariani [ID](#), M. Johnson [ID](#), U. Joshi [ID](#), T. Klijnsma [ID](#), B. Klima [ID](#), K.H.M. Kwok [ID](#), S. Lammel [ID](#), D. Lincoln [ID](#), R. Lipton [ID](#), T. Liu [ID](#), C. Madrid [ID](#), K. Maeshima [ID](#), C. Mantilla [ID](#), D. Mason [ID](#), P. McBride [ID](#), P. Merkel [ID](#), S. Mrenna [ID](#), S. Nahn [ID](#), J. Ngadiuba [ID](#), D. Noonan [ID](#), S. Norberg, V. Papadimitriou [ID](#), N. Pastika [ID](#), K. Pedro [ID](#), C. Pena⁸³ [ID](#), F. Ravera [ID](#), A. Reinsvold Hall⁸⁴ [ID](#), L. Ristori [ID](#), M. Safdari [ID](#), E. Sexton-Kennedy [ID](#), N. Smith [ID](#), A. Soha [ID](#), L. Spiegel [ID](#), S. Stoynev [ID](#), J. Strait [ID](#), L. Taylor [ID](#), S. Tkaczyk [ID](#), N.V. Tran [ID](#), L. Uplegger [ID](#), E.W. Vaandering [ID](#), I. Zoi [ID](#)

University of Florida, Gainesville, Florida, USA

C. Aruta [ID](#), P. Avery [ID](#), D. Bourilkov [ID](#), P. Chang [ID](#), V. Cherepanov [ID](#), R.D. Field, E. Koenig [ID](#),

M. Kolosova , J. Konigsberg , A. Korytov , K. Matchev , N. Menendez , G. Mitselmakher , K. Mohrman , A. Muthirakalayil Madhu , N. Rawal , S. Rosenzweig , Y. Takahashi , J. Wang

Florida State University, Tallahassee, Florida, USA

T. Adams , A. Al Kadhim , A. Askew , S. Bower , V. Hagopian , R. Hashmi , R.S. Kim , S. Kim , T. Kolberg , G. Martinez, H. Prosper , P.R. Prova, M. Wulansatiti , R. Yohay , J. Zhang

Florida Institute of Technology, Melbourne, Florida, USA

B. Alsufyani, M.M. Baarmand , S. Butalla , S. Das , T. Elkafrawy⁸⁵ , M. Hohlmann , E. Yanes

University of Illinois Chicago, Chicago, Illinois, USA

M.R. Adams , A. Baty , C. Bennett, R. Cavanaugh , R. Escobar Franco , O. Evdokimov , C.E. Gerber , M. Hawksworth, A. Hingrajiya, D.J. Hofman , J.h. Lee , D. S. Lemos , A.H. Merrit , C. Mills , S. Nanda , G. Oh , B. Ozek , D. Pilipovic , R. Pradhan , E. Prifti, T. Roy , S. Rudrabhatla , M.B. Tonjes , N. Varelas , M.A. Wadud , Z. Ye , J. Yoo

The University of Iowa, Iowa City, Iowa, USA

M. Alhusseini , D. Blend, K. Dilsiz⁸⁶ , L. Emediato , G. Karaman , O.K. Köseyan , J.-P. Merlo, A. Mestvirishvili⁸⁷ , O. Neogi, H. Ogul⁸⁸ , Y. Onel , A. Penzo , C. Snyder, E. Tiras⁸⁹

Johns Hopkins University, Baltimore, Maryland, USA

B. Blumenfeld , L. Corcodilos , J. Davis , A.V. Gritsan , L. Kang , S. Kyriacou , P. Maksimovic , M. Roguljic , J. Roskes , S. Sekhar , M.V. Srivastav , M. Swartz , R. Wang

The University of Kansas, Lawrence, Kansas, USA

A. Abreu , L.F. Alcerro Alcerro , J. Anguiano , S. Arteaga Escatel , P. Baringer , A. Bean , Z. Flowers , D. Grove , J. King , G. Krintiras , M. Lazarovits , C. Le Mahieu , J. Marquez , M. Murray , M. Nickel , M. Pitt , S. Popescu⁹⁰ , C. Rogan , C. Royon , R. Salvatico , S. Sanders , C. Smith , G. Wilson

Kansas State University, Manhattan, Kansas, USA

B. Allmond , R. Guju Gurunadha , A. Ivanov , K. Kaadze , Y. Maravin , J. Natoli , D. Roy , G. Sorrentino

University of Maryland, College Park, Maryland, USA

A. Baden , A. Belloni , J. Bistany-riebman, Y.M. Chen , S.C. Eno , N.J. Hadley , S. Jabeen , R.G. Kellogg , T. Koeth , B. Kronheim, Y. Lai , S. Lascio , A.C. Mignerey , S. Nabili , C. Palmer , C. Papageorgakis , M.M. Paranjpe, L. Wang

Massachusetts Institute of Technology, Cambridge, Massachusetts, USA

J. Bendavid , I.A. Cali , P.c. Chou , M. D'Alfonso , J. Eysermans , C. Freer , G. Gomez-Ceballos , M. Goncharov, G. Grossos, P. Harris, D. Hoang, D. Kovalskyi , J. Krupa , L. Lavezzi , Y.-J. Lee , K. Long , C. Mcginn, A. Novak , M.I. Park , C. Paus , C. Roland , G. Roland , S. Rothman , G.S.F. Stephans , Z. Wang , B. Wyslouch , T. J. Yang

University of Minnesota, Minneapolis, Minnesota, USA

B. Crossman , B.M. Joshi , C. Kapsiak , M. Krohn , D. Mahon , J. Mans 

B. Marzocchi , R. Rusack , R. Saradhy , N. Strobbe 

University of Nebraska-Lincoln, Lincoln, Nebraska, USA

K. Bloom , D.R. Claes , G. Haza , J. Hossain , C. Joo , I. Kravchenko , J.E. Siado , W. Tabb , A. Vagnerini , A. Wightman , F. Yan , D. Yu

State University of New York at Buffalo, Buffalo, New York, USA

H. Bandyopadhyay , L. Hay , H.w. Hsia , I. Iashvili , A. Kalogeropoulos , A. Kharchilava , M. Morris , D. Nguyen , S. Rappoccio , H. Rejeb Sfar , A. Williams , P. Young

Northeastern University, Boston, Massachusetts, USA

G. Alverson , E. Barberis , J. Bonilla , J. Dervan , Y. Haddad , Y. Han , A. Krishna , J. Li , M. Lu , G. Madigan , R. Mccarthy , D.M. Morse , V. Nguyen , T. Orimoto , A. Parker , L. Skinnari , D. Wood

Northwestern University, Evanston, Illinois, USA

J. Bueghly , S. Dittmer , K.A. Hahn , Y. Liu , Y. Miao , D.G. Monk , M.H. Schmitt , A. Taliercio , M. Velasco 

University of Notre Dame, Notre Dame, Indiana, USA

G. Agarwal , R. Band , R. Bucci , S. Castells , A. Das , R. Goldouzian , M. Hildreth , K.W. Ho , K. Hurtado Anampa , T. Ivanov , C. Jessop , K. Lannon , J. Lawrence , N. Loukas , L. Lutton , J. Mariano , N. Marinelli , I. Mcalister , T. McCauley , C. Mcgrady , C. Moore , Y. Musienko¹⁷ , H. Nelson , M. Osherson , A. Piccinelli , R. Ruchti , A. Townsend , Y. Wan , M. Wayne , H. Yockey , M. Zarucki , L. Zygalas

The Ohio State University, Columbus, Ohio, USA

A. Basnet , B. Bylsma , M. Carrigan , L.S. Durkin , C. Hill , M. Joyce , M. Nunez Ornelas , K. Wei , B.L. Winer , B. R. Yates 

Princeton University, Princeton, New Jersey, USA

H. Bouchamaoui , P. Das , G. Dezoort , P. Elmer , A. Frankenthal , B. Greenberg , N. Haubrich , K. Kennedy , G. Kopp , S. Kwan , D. Lange , A. Loeliger , D. Marlow , I. Ojalvo , J. Olsen , A. Shevelev , D. Stickland , C. Tully

University of Puerto Rico, Mayaguez, Puerto Rico, USA

S. Malik 

Purdue University, West Lafayette, Indiana, USA

A.S. Bakshi , S. Chandra , R. Chawla , A. Gu , L. Gutay , M. Jones , A.W. Jung , A.M. Koshy , M. Liu , G. Negro , N. Neumeister , G. Paspalaki , S. Piperov , V. Scheurer , J.F. Schulte , M. Stojanovic , J. Thieman , A. K. Virdi , F. Wang , W. Xie

Purdue University Northwest, Hammond, Indiana, USA

J. Dolen , N. Parashar , A. Pathak 

Rice University, Houston, Texas, USA

D. Acosta , T. Carnahan , K.M. Ecklund , P.J. Fernández Manteca , S. Freed , P. Gardner , F.J.M. Geurts , W. Li , J. Lin , O. Miguel Colin , B.P. Padley , R. Redjimi , J. Rotter , E. Yigitbasi , Y. Zhang

University of Rochester, Rochester, New York, USA

A. Bodek , P. de Barbaro , R. Demina , A. Garcia-Bellido , O. Hindrichs , A. Khukhunaishvili , N. Parmar , P. Parygin⁹¹ , E. Popova⁹¹ , R. Taus 

Rutgers, The State University of New Jersey, Piscataway, New Jersey, USA

B. Chiarito, J.P. Chou , S.V. Clark , D. Gadkari , Y. Gershtein , E. Halkiadakis , M. Heindl , C. Houghton , D. Jaroslawski , S. Konstantinou , I. Laflotte , A. Lath , R. Montalvo, K. Nash, J. Reichert , H. Routray , P. Saha , S. Salur , S. Schnetzer, S. Somalwar , R. Stone , S.A. Thayil , S. Thomas, J. Vora , H. Wang 

University of Tennessee, Knoxville, Tennessee, USA

D. Ally , A.G. Delannoy , S. Fiorendi , S. Higginbotham , T. Holmes , A.R. Kanuganti , N. Karunarathna , L. Lee , E. Nibigira , S. Spanier 

Texas A&M University, College Station, Texas, USA

D. Aebi , M. Ahmad , T. Akhter , O. Bouhali⁹² , R. Eusebi , J. Gilmore , T. Huang , T. Kamon⁹³ , H. Kim , S. Luo , R. Mueller , D. Overton , D. Rathjens , A. Safonov

Texas Tech University, Lubbock, Texas, USA

N. Akchurin , J. Damgov , N. Gogate , V. Hegde , A. Hussain , Y. Kazhykarim, K. Lamichhane , S.W. Lee , A. Mankel , T. Peltola , I. Volobouev 

Vanderbilt University, Nashville, Tennessee, USA

E. Appelt , Y. Chen , S. Greene, A. Gurrola , W. Johns , R. Kunnawalkam Elayavalli , A. Melo , F. Romeo , P. Sheldon , S. Tuo , J. Velkovska , J. Viinikainen 

University of Virginia, Charlottesville, Virginia, USA

B. Cardwell , B. Cox , J. Hakala , R. Hirosky , A. Ledovskoy , C. Neu 

Wayne State University, Detroit, Michigan, USA

S. Bhattacharya , P.E. Karchin 

University of Wisconsin - Madison, Madison, Wisconsin, USA

A. Aravind, S. Banerjee , K. Black , T. Bose , S. Dasu , I. De Bruyn , P. Everaerts , C. Galloni, H. He , M. Herndon , A. Herve , C.K. Koraka , A. Lanaro, R. Loveless , J. Madhusudanan Sreekala , A. Mallampalli , A. Mohammadi , S. Mondal, G. Parida , L. Pétré , D. Pinna, A. Savin, V. Shang , V. Sharma , W.H. Smith , D. Teague, H.F. Tsoi , W. Vetens , A. Warden

Authors affiliated with an institute or an international laboratory covered by a cooperation agreement with CERN

S. Afanasiev , V. Alexakhin , D. Budkouski , I. Golutvin[†] , I. Gorbunov , V. Karjavine , V. Korenkov , A. Lanev , A. Malakhov , V. Matveev⁹⁴ , V. Palichik , V. Perelygin , M. Savina , V. Shalaev , S. Shmatov , S. Shulha , V. Smirnov , O. Teryaev , N. Voytishin , B.S. Yuldashev⁹⁵, A. Zarubin , I. Zhizhin , G. Gavrilov , V. Golovtcov , Y. Ivanov , V. Kim⁹⁴ , P. Levchenko⁹⁶ , V. Murzin , V. Oreshkin , D. Sosnov , V. Sulimov , L. Uvarov , A. Vorobyev[†], Yu. Andreev , A. Dermenev , S. Gninenko , N. Golubev , A. Karneyeu , D. Kirpichnikov , M. Kirsanov , N. Krasnikov , I. Tlisova , A. Toropin , T. Aushev , V. Gavrilov , N. Lychkovskaya , A. Nikitenko^{97,98} , V. Popov , A. Zhokin , R. Chistov⁹⁴ , M. Danilov⁹⁴ , S. Polikarpov⁹⁴ , V. Andreev , M. Azarkin , M. Kirakosyan, A. Terkulov , E. Boos , V. Bunichev , M. Dubinin⁸³ , L. Dudko , A. Ershov , V. Klyukhin , O. Kodolova⁹⁸ , S. Obraztsov , M. Perfilov, V. Savrin , P. Volkov , G. Vorotnikov , V. Blinov⁹⁴, T. Dimova⁹⁴ , A. Kozyrev⁹⁴ , O. Radchenko⁹⁴ , Y. Skovpen⁹⁴ , V. Kachanov , D. Konstantinov , S. Slabospitskii , A. Uzunian , A. Babaev , V. Borshch , D. Druzhkin⁹⁹

Authors affiliated with an institute formerly covered by a cooperation agreement with CERN

V. Chekhovsky, V. Makarenko 

†: Deceased

¹Also at Yerevan State University, Yerevan, Armenia

²Also at TU Wien, Vienna, Austria

³Also at Institute of Basic and Applied Sciences, Faculty of Engineering, Arab Academy for Science, Technology and Maritime Transport, Alexandria, Egypt

⁴Also at Ghent University, Ghent, Belgium

⁵Also at Universidade do Estado do Rio de Janeiro, Rio de Janeiro, Brazil

⁶Also at Universidade Estadual de Campinas, Campinas, Brazil

⁷Also at Federal University of Rio Grande do Sul, Porto Alegre, Brazil

⁸Also at UFMS, Nova Andradina, Brazil

⁹Also at Nanjing Normal University, Nanjing, China

¹⁰Now at The University of Iowa, Iowa City, Iowa, USA

¹¹Also at University of Chinese Academy of Sciences, Beijing, China

¹²Also at China Center of Advanced Science and Technology, Beijing, China

¹³Also at University of Chinese Academy of Sciences, Beijing, China

¹⁴Also at China Spallation Neutron Source, Guangdong, China

¹⁵Now at Henan Normal University, Xinxiang, China

¹⁶Also at Université Libre de Bruxelles, Bruxelles, Belgium

¹⁷Also at an institute or an international laboratory covered by a cooperation agreement with CERN

¹⁸Also at Suez University, Suez, Egypt

¹⁹Now at British University in Egypt, Cairo, Egypt

²⁰Also at Purdue University, West Lafayette, Indiana, USA

²¹Also at Université de Haute Alsace, Mulhouse, France

²²Also at İstinye University, Istanbul, Turkey

²³Also at The University of the State of Amazonas, Manaus, Brazil

²⁴Also at University of Hamburg, Hamburg, Germany

²⁵Also at RWTH Aachen University, III. Physikalisches Institut A, Aachen, Germany

²⁶Also at Bergische University Wuppertal (BUW), Wuppertal, Germany

²⁷Also at Brandenburg University of Technology, Cottbus, Germany

²⁸Also at Forschungszentrum Jülich, Juelich, Germany

²⁹Also at CERN, European Organization for Nuclear Research, Geneva, Switzerland

³⁰Also at Institute of Nuclear Research ATOMKI, Debrecen, Hungary

³¹Now at Universitatea Babes-Bolyai - Facultatea de Fizica, Cluj-Napoca, Romania

³²Also at MTA-ELTE Lendület CMS Particle and Nuclear Physics Group, Eötvös Loránd University, Budapest, Hungary

³³Also at HUN-REN Wigner Research Centre for Physics, Budapest, Hungary

³⁴Also at Physics Department, Faculty of Science, Assiut University, Assiut, Egypt

³⁵Also at Punjab Agricultural University, Ludhiana, India

³⁶Also at University of Visva-Bharati, Santiniketan, India

³⁷Also at Indian Institute of Science (IISc), Bangalore, India

³⁸Also at IIT Bhubaneswar, Bhubaneswar, India

³⁹Also at Institute of Physics, Bhubaneswar, India

⁴⁰Also at University of Hyderabad, Hyderabad, India

⁴¹Also at Deutsches Elektronen-Synchrotron, Hamburg, Germany

⁴²Also at Isfahan University of Technology, Isfahan, Iran

⁴³Also at Sharif University of Technology, Tehran, Iran

⁴⁴Also at Department of Physics, University of Science and Technology of Mazandaran, Behshahr, Iran

- ⁴⁵Also at Department of Physics, Isfahan University of Technology, Isfahan, Iran
⁴⁶Also at Department of Physics, Faculty of Science, Arak University, ARAK, Iran
⁴⁷Also at Helwan University, Cairo, Egypt
⁴⁸Also at Italian National Agency for New Technologies, Energy and Sustainable Economic Development, Bologna, Italy
⁴⁹Also at Centro Siciliano di Fisica Nucleare e di Struttura Della Materia, Catania, Italy
⁵⁰Also at Università degli Studi Guglielmo Marconi, Roma, Italy
⁵¹Also at Scuola Superiore Meridionale, Università di Napoli 'Federico II', Napoli, Italy
⁵²Also at Fermi National Accelerator Laboratory, Batavia, Illinois, USA
⁵³Also at Consiglio Nazionale delle Ricerche - Istituto Officina dei Materiali, Perugia, Italy
⁵⁴Also at Department of Applied Physics, Faculty of Science and Technology, Universiti Kebangsaan Malaysia, Bangi, Malaysia
⁵⁵Also at Consejo Nacional de Ciencia y Tecnología, Mexico City, Mexico
⁵⁶Also at Trincomalee Campus, Eastern University, Sri Lanka, Nilaveli, Sri Lanka
⁵⁷Also at Saegis Campus, Nugegoda, Sri Lanka
⁵⁸Also at National and Kapodistrian University of Athens, Athens, Greece
⁵⁹Also at Ecole Polytechnique Fédérale Lausanne, Lausanne, Switzerland
⁶⁰Also at Universität Zürich, Zurich, Switzerland
⁶¹Also at Stefan Meyer Institute for Subatomic Physics, Vienna, Austria
⁶²Also at Laboratoire d'Annecy-le-Vieux de Physique des Particules, IN2P3-CNRS, Annecy-le-Vieux, France
⁶³Also at Near East University, Research Center of Experimental Health Science, Mersin, Turkey
⁶⁴Also at Konya Technical University, Konya, Turkey
⁶⁵Also at Izmir Bakircay University, Izmir, Turkey
⁶⁶Also at Adiyaman University, Adiyaman, Turkey
⁶⁷Also at Bozok Universitetesi Rektörlüğü, Yozgat, Turkey
⁶⁸Also at Marmara University, Istanbul, Turkey
⁶⁹Also at Milli Savunma University, Istanbul, Turkey
⁷⁰Also at Kafkas University, Kars, Turkey
⁷¹Now at Istanbul Okan University, Istanbul, Turkey
⁷²Also at Hacettepe University, Ankara, Turkey
⁷³Also at Erzincan Binali Yıldırım University, Erzincan, Turkey
⁷⁴Also at Istanbul University - Cerrahpasa, Faculty of Engineering, Istanbul, Turkey
⁷⁵Also at Yildiz Technical University, Istanbul, Turkey
⁷⁶Also at Vrije Universiteit Brussel, Brussel, Belgium
⁷⁷Also at School of Physics and Astronomy, University of Southampton, Southampton, United Kingdom
⁷⁸Also at IPPP Durham University, Durham, United Kingdom
⁷⁹Also at Monash University, Faculty of Science, Clayton, Australia
⁸⁰Also at Università di Torino, Torino, Italy
⁸¹Also at Bethel University, St. Paul, Minnesota, USA
⁸²Also at Karamanoğlu Mehmetbey University, Karaman, Turkey
⁸³Also at California Institute of Technology, Pasadena, California, USA
⁸⁴Also at United States Naval Academy, Annapolis, Maryland, USA
⁸⁵Also at Ain Shams University, Cairo, Egypt
⁸⁶Also at Bingöl University, Bingöl, Turkey
⁸⁷Also at Georgian Technical University, Tbilisi, Georgia
⁸⁸Also at Sinop University, Sinop, Turkey

⁸⁹Also at Erciyes University, Kayseri, Turkey

⁹⁰Also at Horia Hulubei National Institute of Physics and Nuclear Engineering (IFIN-HH), Bucharest, Romania

⁹¹Now at another institute or international laboratory covered by a cooperation agreement with CERN

⁹²Also at Texas A&M University at Qatar, Doha, Qatar

⁹³Also at Kyungpook National University, Daegu, Korea

⁹⁴Also at another institute or international laboratory covered by a cooperation agreement with CERN

⁹⁵Also at Institute of Nuclear Physics of the Uzbekistan Academy of Sciences, Tashkent, Uzbekistan

⁹⁶Also at Northeastern University, Boston, Massachusetts, USA

⁹⁷Also at Imperial College, London, United Kingdom

⁹⁸Now at Yerevan Physics Institute, Yerevan, Armenia

⁹⁹Also at Universiteit Antwerpen, Antwerpen, Belgium